Muonium states and dynamics

S F J Cox

ISIS Pulsed Muon Facility, Rutherford Appleton Laboratory, and
University College London.

1 Muon sites and electronic structure

1.1 Introduction

This section concerns the sites adopted by positive muons implanted in different materials. It examines how the nature of the material determines the muons' local environment, as relevant to μSR studies. That is, it examines what needs to be known of the muon or muonium chemical state in order to understand the evolution of the spin states. The guiding principle is that muons, like protons, cannot remain as free particles once they are thermalised in matter, whether in gases, liquids or solids. They seek to lower their energy by association with electrons. They do this in inert materials by the formation of muonium, *i.e.* by binding a single electron to form a hydrogen-like atom, and in more reactive hosts by becoming chemically bound into the structure of the lattices or molecules. As a general rule, the chemistry of protons and atomic hydrogen may be taken as a guide to the states reached by muons and muonium, provided proper account is taken of the larger zero-point energy of the muon when confined or bound.

The relevant properties of atomic muonium are given, followed by a description of how these are modified in various hosts, dielectric, molecular and metallic. (The states specific to semiconductors are the subject of Section 2 The various possibilities are well illustrated by the muonium states observed in the different allotropes of carbon. More detailed accounts of many of the topics, together with original references, are to be found in the review article "Implanted muon studies in condensed matter science" (Cox, 1987). The present account serves to introduce aspects which are developed in other lectures at the school.

1.2 Muonium

Atomic muonium is formed in a variety of inert materials, gases, liquids and solids. The initially energetic incoming muon picks up an electron at some stage during the course of

its thermalisation (Storchak, this volume). The closest approximation to the free-atom state is achieved for muonium formed at low pressure in rare gases (except He, which has a larger ionisation potential than Mu), or formed in thin foils or fine powder production targets and ejected into a vacuum space beyond. This serves for the determination of the fundamental spectroscopic parameters, notably the energy level separations depicted as wide arrows in Figure 1 (Jungmann, this volume).

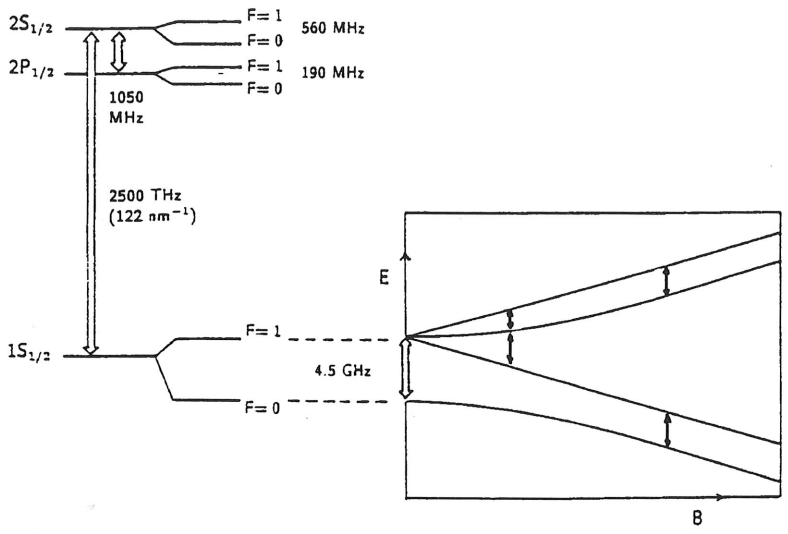

Figure 1. *Energy levels for vacuum-state muonium.*

1.2.1 Hyperfine interaction (isotropic)

We focus attention on the electronic ground state, described by a 1s hydrogenic orbital. The electron spin **S** and muon spin **I** are coupled by a scalar product interaction:

$$\mathcal{H} = Ah\,\mathbf{S}\cdot\mathbf{I}, \tag{1}$$

variously known as the hyperfine, Fermi or contact interaction. It results from the magnetic interaction between muon and electron which has the property – for a spherical or s–state electronic distribution – that it sums to zero except where the electronic wavefunction actually overlaps the nucleus. This is the origin of the name "contact" term and it implies that the *hyperfine constant*, A, is a measure of the electron density at the nucleus:

$$A \propto |\psi(0)|^2. \tag{2}$$

The hyperfine constant is usually expressed in units of frequency. The free-atom or vacuum-state value for muonium is

$$A_0 = 4.46\text{GHz}, \tag{3}$$

which is greater than that for protium by the ratio (3.18) of the magnetic moments of muon and proton. This implies essentially the same electron density (*i.e.* spin density) at the nuclei, confirming the notion of muonium as a pseudo-isotope of hydrogen and serving as a starting point for examining the changes which arise on incorporation into materials.

1.2.2 Muonium in dielectrics

The Breit-Rabi diagram

Equation 1 is the spin-Hamiltonian for muonium (in its electronic ground state) in null external field. Adding the electron and muon Zeeman energies in an applied magnetic field generates the energy-level scheme shown framed in Figure 1. This is known as the *Breit-Rabi diagram*, originally conceived for atomic hydrogen (*i.e.* protium). (Expressions for the eigenvalues and eigenstates as functions of hyperfine constant and magnetic field are given in standard magnetic resonance texts, *e.g* Atherton (1993). See also Section 3 and Roduner, this volume.) Characteristic frequencies corresponding to the transitions between the various states (the thin arrows in Figure 1) appear in the muon spin rotation or rf-resonance spectra, with intensities reflecting the field-dependent selection rules. The hyperfine constant may be deduced from these frequencies, either directly from the sum of the two frequencies in the high-field spectrum or, indirectly and less precisely, from the difference of the two frequencies in low field (the so-called *triplet muonium* spectrum). The hyperfine constant appears in the energy level diagram as the zero-field splitting between the singlet and triplet so that direct observation of "hyperfine oscillations" at this frequency provides the most precise determination, provided that (a) there are not too many additional zero-field splittings (see below) and (b) an apparatus of exceptional timing resolution is available.

Influence of the medium

In inert and non-conducting solid media, muonium can exist in a form which closely resembles the atomic state, but which is located in the interstitial spaces of the lattice. The term "trapped atom" is often used but is somewhat misleading, since muonium is often free to diffuse, moving between interstitial sites. In some alkali fluorides its hyperfine constant is slightly higher than the vacuum-state value, as though the electronic wavefunction were compressed, increasing its amplitude at the muon. More commonly, the hyperfine constant is lower – in the semiconductors considerably lower – than in the free atom. For interstitial hydrogen a similar small variation was known in the oxides and halides, traditional hosts for ESR studies of defect centres, but the much larger reduction for the semiconductors was only discovered by μSR. Values for various hosts are expressed in Figure 2 as a fraction of the free atom value or *spin density.* They show a broad correlation with band-gap. (The correlation can be justified in a *molecular orbital* description if all the centres, with the evident exception of those in the cuprous halides, have a similar character: the greater the disparity between the levels of the states to be mixed, the smaller is the degree of mixing *i.e.* the more the muonium retains its atomic character: see Cox and Symons, 1986).

Super-hyperfine interaction

The reduction of the hyperfine constant for muonium in solids implies some dilation of the electronic wave function by mixing with neighbouring atomic orbitals: The unpaired

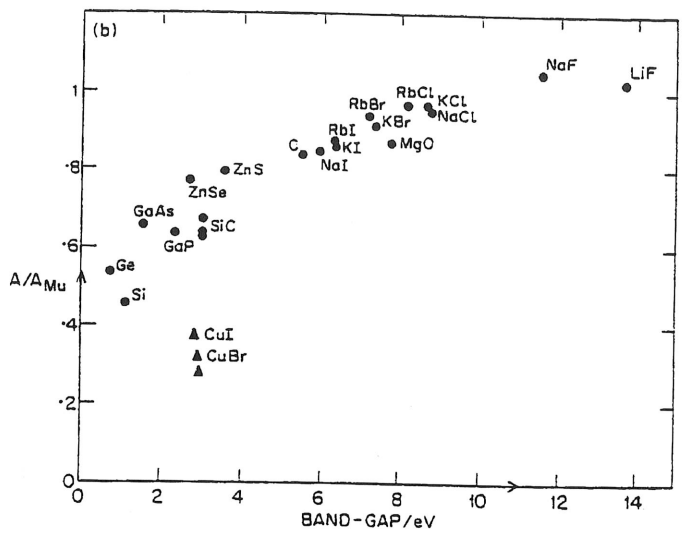

Figure 2. *Variation of the hyperfine constant with band-gap for isotropic muonium centres in various hosts (Cox, 1987).*

electron occupies a molecular orbital:

$$\psi = \alpha_s \psi_s + \sum_i \alpha_i \psi_i, \tag{4}$$

i.e. a linear combination of the muonium 1s orbital centred on the muon and appropriate atomic orbitals centred on neighbouring nuclei. The corresponding (zero-field) spin Hamiltonian, including the neighbouring nuclear or super-hyperfine constants a_i, becomes

$$\mathcal{H}/h = A\,\mathbf{S}\cdot\mathbf{I} + \sum_i a_i\,\mathbf{S}\cdot\mathbf{J}_i, \tag{5}$$

so that the spin-density on the muon (*e.g.* as reported in Figure 2) is given by

$$\alpha_s^2 = A/A_0. \tag{6}$$

Equations 4 and 5 are also appropriate to determining the spin densities "leaking" onto the surrounding atoms (represented by the square of each coefficient α_i); for dipolar nuclei, these can be measured by *level crossing resonance* (LCR) providing the interstitial muonium is not diffusing rapidly. A particularly beautiful spectrum is shown in Figure 3 for one of the cuprous halides, from which the muonium site may be assigned to the centre of the interstitial cage defined by four Cu^+ nearest neighbours. (There are in fact two muonium states with slightly different hyperfine constants in CuCl. The LCR spectra show that the muonium site is the same for each, apparently one with and one without an associated local distortion of the lattice. This is one of several examples of *meta-stability* in muonium dynamics.) The nuclear or super-hyperfine constants a_i are determined from the positions of the resonances (Roduner, this volume) so that the degree of mixing can

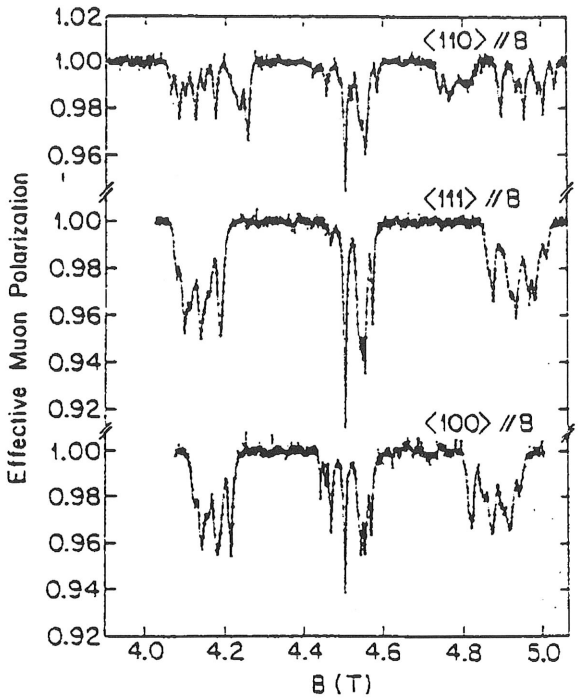

Figure 3. *Level crossing resonances for an isotropic muonium centre in CuCl (Schneider, 1990).*

be determined by the ratio of these to the intrinsic atomic hyperfine constants A_i for the respective atoms (Morton and Preston, 1978):

$$\alpha_i^2 = a_i/A_i. \tag{7}$$

1.2.3 Hyperfine interaction (anisotropic)

Axial symmetry

If the cavity containing the muonium atom goes from cubic or spherical symmetry to lower symmetry, the electron wavefunction may develop a degree of anisotropy to match. The case of axial symmetry is illustrated in Figure 4 for muonium trapped *inside* the cages of the fullerene molecules – the *endohedral* states denoted Mu@C_{60} and Mu@C_{70} (Prassides *et al.* 1992).

In effect, the muonium atom is polarised, which may be described as an admixture of 2p(Mu) orbital:

$$\psi = \alpha_s\psi_s + \alpha_p\psi_p. \tag{8}$$

The admixture depends on the muon's position inside the cage, so that the ellipsoidal electron density is given by the mean square admixture, averaged over the muon's zero-

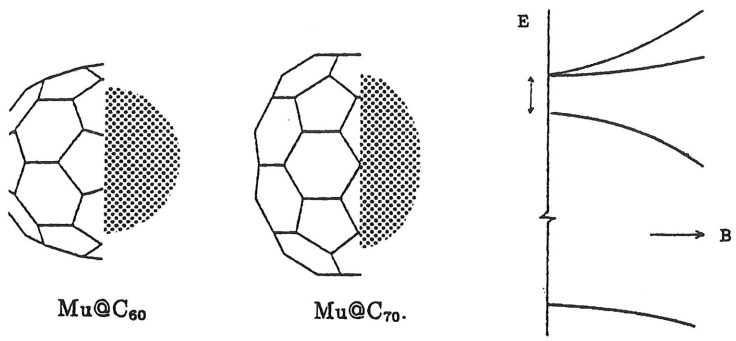

Figure 4. *Contours of electronic density for muonium inside C_{60} and (somewhat exaggerated) C_{70} and the additional zero-field energy splitting for axial asymmetry.*

point motion (Claxton, 1995).

The muon-electron hyperfine interaction then becomes a tensor quantity, with different components perpendicular and parallel to the molecular axis:

$$\mathcal{H}/h = A_\perp(I_xS_x + I_yS_y) + A_\parallel I_zS_z. \tag{9}$$

These components are the observable quantities, deduced from the orientation dependence of the μSR spectrum, but they are usefully decomposed into a combination of an isotropic term and a traceless dipolar term. Since the dipolar interaction usually has an angular dependence $B(3\cos^2\theta - 1)$, *i.e.* has principal values $(-B, -B, 2B)$, we have

$$\mathcal{H}/h = (A_{\rm iso} - B)(I_xS_x + I_yS_y) + (A_{\rm iso} + 2B)I_zS_z, \tag{10}$$

with

$$A_{\rm iso} = \frac{1}{3}(A_\parallel + 2A_\perp), \tag{11}$$

$$B = \frac{1}{3}(A_\parallel - A_\perp). \tag{12}$$

The muonium s-character is given by

$$\alpha_s^2 = A_{\rm iso}/A_o \tag{13}$$

with $A_0 = 4.46$GHz (this is equivalent to Equation 6); the p–character is

$$\alpha_p^2 = B/B_0 \tag{14}$$

with $B_0 = 18.6$MHz, as expected for the muon-electron dipolar interaction for a pure $2p_z$ orbital. (See *e.g.* Prassides *et al.* 1992, but beware different numerical factors in the definitions used by different authors!) The dipolar parameter B can be obtained from the angular variation of the muon spin rotation spectrum, from the width and shape of level-crossing resonances and, in favourable cases, more directly from the appearance of an oscillation at the relatively low frequency $|A_\parallel - A_\perp|/2 = 3B/2$ in the zero-field spectrum.

This is observable if additional splittings due to nuclear super-hyperfine interactions are absent.

A small degree of anisotropy of the hyperfine tensor for muonium in quartz and in ice may also be described in these terms. The overall axial anisotropy in these materials appears to result from diffusion along tube-like interstitial channels. Diffusion also causes a modulation of lower-symmetry components of the electron-muon hyperfine interaction (*e.g.* in quartz) or of the interaction with neighbouring spins (*e.g.* the protons in ice) and may be studied *via* muon spin relaxation in longitudinal field (Section 3). A particularly extreme example of axial anisotropy is exhibited by certain muonium states in tetrahedral semiconductors (Section 2).

Full anisotropy

Some muonium centres show rhombic symmetry, *i.e.* a hyperfine tensor with three distinct principal values:

$$\mathcal{H}/h = A_{xx}I_xS_x + A_{yy}I_yS_y + A_{zz}I_zS_z. \tag{15}$$

This is the case in quartz at very low temperature, where the muonium atom is no longer diffusing (Brewer *et al.* 1981). All degeneracy is removed in the triplet state and the zero-field spectrum shows frequencies $|A_{xx} - A_{yy}|/2$, $|A_{xx} - A_{zz}|/2$ and $|A_{yy} - A_{zz}|/2$. A very few organic radicals (those of low symmetry with the muon immediately adjacent to the radical centre – see below) should exhibit a dipolar tensor of the form $(0, -B, B)$ so that for these, Equation 15 becomes

$$\mathcal{H}/h = A_{\rm iso}I_xI_y + (A_{\rm iso} - B)I_yS_y + (A_{\rm iso} + B)I_zS_z \tag{16}$$

and the relations 11 and 12 are modified accordingly.

1.3 Organic radicals

A chemical reaction which is well known for atomic hydrogen is addition at multiple bonds in *unsaturated* organic compounds. Addition to the carbon-carbon double bond of ethylene, for instance, forms the *ethyl radical*, which is known to ESR spectroscopy:

$$\mathrm{H_2C{=}CH_2} \;+\; \dot{\mathrm{H}} \;\rightarrow\; \dot{\mathrm{C}}\mathrm{H_2}\text{–}\mathrm{CH_3} \tag{17}$$

In this notation the dot is used to emphasise the existence of the unpaired electron spin, the term *radical* or *free radical* being used to to denote open-shell or paramagnetic molecules. (The ethyl radical has an electronic doublet ground state and, in common with all radicals discussed below, a g-factor close to 2, indicating that the electronic spin is the dominant contribution to the magnetic moment. An exception would be the muonated hydroxyl radical, ȮMu.)

Muonium does likewise, forming the *muonated* or *muonium-substituted* ethyl radical. This is the net result of implanting positive muons in ethylene, liquid or gas:

$$\mathrm{H_2C{=}CH_2} \;+\dot{\mathrm{M}}\mathrm{u} \;\rightarrow\; \dot{\mathrm{C}}\mathrm{H_2}\text{–}\mathrm{CH_2Mu}. \tag{18}$$

In these paramagnetic species, there is again a hyperfine interaction between the muon and the unpaired electron. It gives rise to a characteristic 2-line spectrum in high field, as

in Figure 5. The hyperfine constant is the sum of these two frequencies; it is less than 10% of that for atomic muonium, since the wavefunction of the unpaired electron is centred not on the muon but elsewhere in the molecule – on the carbon atom known as the radical centre. Equations 4–14 for the molecular orbital descriptions, spin Hamiltonians and spin densities can all be used for these open-shell molecules, as for the muonium defect centres in insulators (Section 1.2 above) and in semiconductors (Section 2).

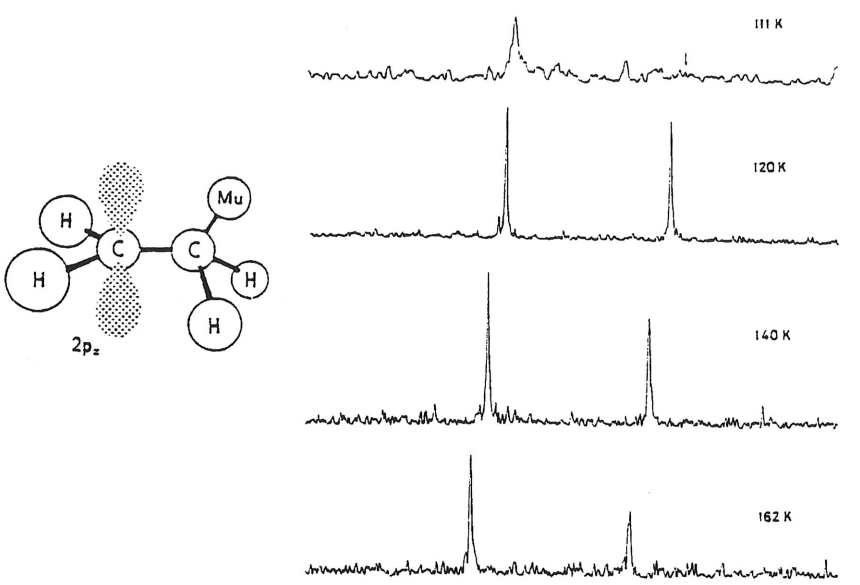

Figure 5. *Structure of $CH_2.CH_2Mu$ radical, with major spin density on one carbon atom, and its (Fourier transform) μSR spectra in liquid ethylene. Anisotropy broadening is apparent near the freezing point (Ramos et al. 1984).*

Addition reactions open the double bond, saturating one carbon atom and leaving an unpaired electron spin located, largely, on the other. Roughly stated, the addition reaction leaves a *dangling bond* on this atom. The dot-notation in the formula $\dot{C}H_2$–CH_2Mu and the sketch showing the unpaired electron occupying a $2p_z$ orbital on this carbon atom, the " radical centre", give a rather misleading picture of total localisation. This is in fact just the leading term of the LCAO (Equation 4), with the molecular orbital extending over the entire molecular frame. The contact interaction (Equation 11) in such radicals again represents spin density on the muon, now obtained as the difference between up-spin and down-spin electron densities taken over all occupied molecular orbitals. (That is, it includes any indirect or negative contributions from spin-polarisation of the doubly-occupied bonding orbitals.) It is typically 10–20% greater than the spin density on a proton in the same position (in this case the CH_3 or β–protons of the "ordinary" ethyl radical), this fascinating isotope effect being largely due to the greater zero-point energy of

the muon (Roduner, this volume). The temperature dependence of the hyperfine constant is informative on low-lying internal modes of vibration (Ramos *et al.* 1984; Buttar *et al.* 1990; Webster and Buttar, 1996). In the muonated ethyl radical, for instance, the most important is the torsional libration or hindered rotation about the C–C bond.

In solid or frozen hosts, the anisotropy term (Equation 12) represents the net *dipolar* interaction with the unpaired electron distribution. It can be seen broadening the spectral lines in Figure 5 close to the freezing point. For muonium addition at a double bond, the muon is invariably placed in the β position, *i.e.* with an intervening atom between it and the radical centre. Dipolar tensors of the form ($2B$, $-B$, $-B$) are then appropriate, as in Equation 10, with the parameter B typically a few tens of MHz. Rather few radicals with α muons, immediately adjacent to the radical centre, are known. For those of low symmetry, *e.g.* derivatives of $\dot{C}H_2Mu$, the muonated methyl (Addison-Jones *et al.* 1994), the special form (0, $-B$, B) should apply, as in Equation 16. In either case, the dipolar tensor is traceless and has the property of being averaged to zero by fast tumbling of the molecules in the fluid phases. Liquid and gas phase spectra therefore give the isotropic term directly. In high-field spectra it is just the sum of the two frequencies, as in Figure 5. The amount of spin density which "leaks" onto each of the other dipolar nuclei – in the ethyl radical onto the α and β protons (Percival *et al.* 1989) – can be determined by level-crossing resonance (Roduner, this volume); this is analogous to the determination of nuclear or super-hyperfine interactions for the muonium centres in solids (Section 1.2).

Radical formation by muonium addition at multiple bonds involving oxygen, nitrogen and sulphur is also known. Many of the radicals are highly reactive transient species, and μSR detection serves to determine their chemical lifetimes, in studies of reaction kinetics (Roduner, this volume). Gas phase studies of complex radicals by conventional ESR prove impossible, so here μSR studies of the muonium-substituted counterparts are particularly noteworthy (*e.g.* Percival *et al.* 1989).

Another favorite and much studied example is the muonium-substituted *cyclohexadienyl* radical, formed in benzene (Roduner, this volume):

$$C_6H_6 + Mu \rightarrow C_6H_6Mu. \tag{19}$$

Conjugation of the bonds results in extensive delocalisation of the electronic spin around the ring, the spin densities on each carbon atom being elegantly mapped out by the ^{13}C level-crossing resonances in an isotopically enriched sample (Kiefl *et al.* 1988).

The species $C_{60}Mu$, the muonium *adduct* of C_{60} fullerene, is also worth a special mention. It is the analogue of the monohydride of C_{60} but has the distinction of having been detected in μSR studies *before* $C_{60}H$ was recognised in ESR studies. $C_{60}Mu$ is quite different from the endohedral complex, Mu@C_{60}. (The endohedral state, Mu@C_{60}, represented in Figure 4, provides another remarkable example of metastability in muonium studies: some potential barrier prevents reaction with the cage structure from inside. Its signal coexists with that of $C_{60}Mu$ in the μSR spectrum.) $C_{60}Mu$ is the result of external addition, muonium attacking one of the double bonds much as in the reaction with ethylene, so that the muon is located outside the fullerene cage, covalently bound to a single (saturated) carbon atom. Major spin density resides on the adjacent carbon atom but some leaks over the entire sphere by the small degree of conjugation. Amazingly, this distribution too has been mapped with ^{13}C resonances in a suitably enriched, and presumably very expensive, sample (Percival *et al.* 1995)!

The transverse-field muon spin rotation spectrum for $C_{60}Mu$ is shown in Figure 6. It is remarkable in showing strong narrow lines over a considerable temperature range, even in *solid state, powder* samples of C_{60}. For the other muonated radicals the solid state spectra, unless from single-crystal samples, are broadened and weakened by the hyperfine anisotropy, often beyond detection. In solid C_{60}, however, the individual molecules can reorient whilst their centres of mass remain fixed on the lattice structure. The result is a progressive *motional narrowing* of the μSR line-widths in the phase between 90 and 260K, from which the correlation time for the reorientation can be deduced. Extreme narrowing corresponding to liquid-like rotational diffusion is seen in the (still solid) phase above 260K. The spectra for solid C_{60} may be compared with those for liquid ethylene (Figure 5). The reorientation can also be studied by its effect on level-crossing resonance (Roduner, this volume) and *via* spin-lattice relaxation (Section 3).

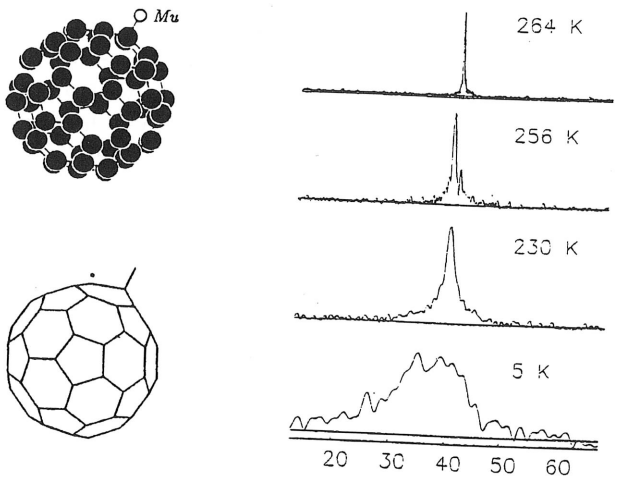

Figure 6. *The radical $C_{60}Mu$ and its μSR spectra (lower frequency line only) showing motionally narrowed lines in the plastic phases of solid C_{60} (Kiefl et al. 1992).*

1.4 Muons in diamagnetic states and closed shell molecules

Again, we use proton and hydrogen chemistry as a guide to the states expected of muons and muonium.

1.4.1 Protonation of bases

Protons are known to "stick" to to lone electron pairs such as commonly exist on oxygen or nitrogen, in the process known as *protonation.* Positive muons are expected to do likewise and add, for instance, to water:

$$H_2O + \mu^+ \rightarrow H_2OMu^+, \tag{20}$$

or to a nitrogen molecule:

$$N_2 + \mu^+ \rightarrow N_2Mu^+. \tag{21}$$

Amazingly, the positive muon can even polarise noble-gas atoms sufficiently to form a molecule ion (Arseneau *et al.* 1988), *e.g:*

$$\mathrm{Ne} + \mu^+ \rightarrow \mathrm{NeMu}^+. \tag{22}$$

The notation (though not universally adopted) is worth underlining here: it is useful to reserve Greek μ^+ for the free particle, or the energetic particle on entry into the sample, and to use Roman Mu^+ for the positive ion after thermalisation, to emphasise that it is always in some chemical association with the host.

In many materials, muons which did not pick up an electron promptly or epithermally, remain chemically stable as a Mu^+ ion. They can also subsequently attract and capture a radiolytic electron, thereby getting a second chance to form muonium if the mobilities are favourable (Storchak, this volume). In the case of water, one of the $\mathrm{H_2OMu}^+$ protons can instead change its allegiance, with the net result that the charge migrates away to leave muonium substituted in a neutral molecule (Percival *et al.* 1978):

$$\mathrm{H_2OMu}^+ + \mathrm{H_2O} \rightarrow \mathrm{HMuO} + \mathrm{H_3O}^+. \tag{23}$$

1.4.2 Identification of diamagnetic states

The products of reactions such as (20–22), whether ionic or neutral, are all *closed shell, i.e. diamagnetic.* There is no unpaired electron in the vicinity of the muon, and therefore no hyperfine interaction. The same is true for the muonium states in semiconductors which are charged rather than neutral (*i.e.* Mu^+ mimicking the interstitial proton and Mu^- mimicking the hydride ion) or which are paired with other impurities or dopants. The muon spin rotation spectrum for such species shows a single line at a frequency close to the muon Larmor frequency appropriate to the applied field. There is in principle a small *chemical shift*, due to diamagnetic shielding currents in the molecule, but these have only been measured in a few favourable cases. (RF resonance at high fields offers the best promise for chemical shift measurements but the muon lifetime, as well as the RF power necessary, set limits on resolution.)

In crystalline materials, the sites of diamagnetic states may often be determined from the orientation dependence of the transverse field μSR linewidth and occasionally from the form of the zero-field relaxation function. The $(\mathrm{F–Mu–F})^-$ ion, for instance, shows a particularly distinctive zero field relaxation (Brewer *et al.* 1986).

When the muon is located immediately adjacent to a quadrupolar nucleus ($J > 1/2$), resonant cross-relaxation can provide a means of identification. These experiments use a longitudinal field to tune the muon Zeeman energy to match the combined Zeeman and quadrupolar energy on the neighbouring nucleus; the muons then lose polarisation by *flip-flop* transitions with their neighbours, as illustrated in Figure 7.

Using total energy level diagrams, the polarisation transfer can be seen to result from mixing of the muon and nuclear spin states at the so-called level crossings – whence the terms *level crossing resonance* (LCR) or *avoided level crossing* (ALC) (Roduner, this volume). Since the lifting of degeneracy by mixing of the individual spin states is a prerequisite to observation of the resonance, purists prefer to call it ALC rather than LCR, but both terms are in common usage. For these diamagnetic states, it is the muon-nuclear

dipolar interaction which mixes the spin states; the cross-relaxation is rather slow and the resonances can be hard to detect. (For paramagnetic states, discussed in Sections 1.2 and 1.3, the separate muon and nuclear hyperfine interactions with the unpaired electron causes much faster cross-relaxation and stronger resonances.)

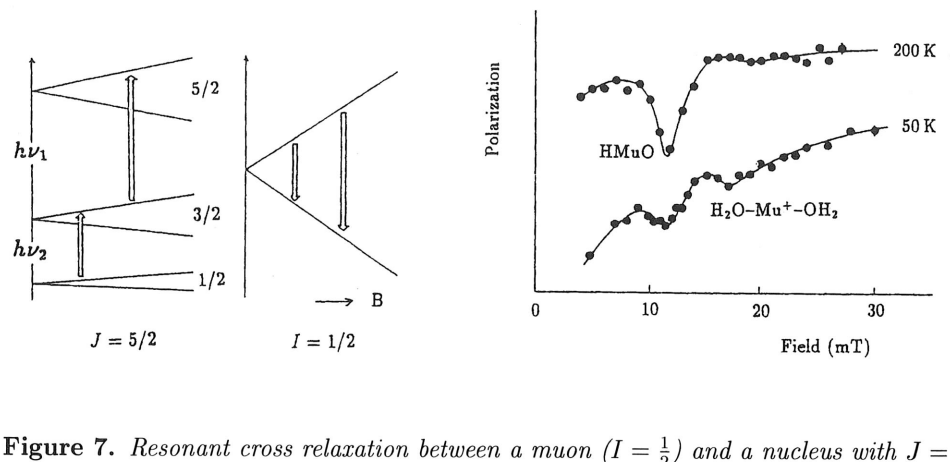

Figure 7. *Resonant cross relaxation between a muon ($I = \frac{1}{2}$) and a nucleus with $J = \frac{5}{2}$ (e.g. ^{17}O) and LCR spectra (Cox, 1992) for ice enriched with $H_2\,^{17}O$.*

The quadrupolar LCR technique requires solid samples, but not necessarily single-crystals, since the spectra are only weakly dependent on orientation. The positions of the resonances provide a measurement of the quadrupole energy splittings which are characteristic of the molecular species. Addition to oxygen and nitrogen as in reactions (20–22) has been demonstrated in this way, and the method applied to characterise muon sites in the oxide superconductors. The spectra in Figure 7 are for ice, with resonances assigned to the substituted molecules HMuO and to the ionic intermediary, thought to be muons trapped at a defect in the hydrogen-bonded network. In semiconductors, the hydride-ion analogue Mu^- has been confirmed by LCR with both Ga and As nuclei in GaAs. Many metals have quadrupolar nuclei so LCR determinations of electric field gradients is in principle a valuable test of screening theory (Section 1.5.1). To date, resonances have been detected for the diamagnetic states in the metallic elements Cu (spin $\frac{3}{2}$), Al (spin $\frac{5}{2}$) and, with difficulty, in Nb (spin $\frac{9}{2}$).

1.5 Muons in metals

1.5.1 Screening

Muonium is not seen in simple metals. This seems paradoxical, in that conduction electrons are always at hand, apparently available to be picked up by the muon. In fact the conduction electron density is too high to allow a bound state with a single electron to be formed. The density of these mobile charges adjusts in response to the muon's presence to screen its Coulomb potential. The muonium binding energy is reduced, not exactly to zero, but to such a shallow level that the lifetime broadening exceeds its depth. Electrons hop on and off the muon, so to speak, in rapid succession. Some of the electrons have

spin-up, some spin-down. In magnetic metals in their ordered state, the conduction electron polarisation can be considerable and their contact interaction can be a significant contribution to the effective field felt by the muon. In diamagnetic metals the interaction is observed as a *Knight shift* – a small proportional change in the muon Larmor frequency from the value appropriate to the externally applied field (Schenck, this volume).

1.5.2 The small polaron state

The muon site in metals is usually interstitial and the same as that adopted by the screened-proton state of hydrogen in metals. The analogy makes implanted muon studies invaluable in modelling certain aspects of the behaviour of hydrogen in metals, especially in metals such as copper where hydrogen itself is too insoluble to be studied by conventional techniques.

The local accumulation of conduction electron density largely screens the muon's positive charge within a distance comparable with the interatomic spacing. Since the screening is not perfect, neighbouring ion cores are slightly repelled, producing a local elastic distortion on relaxation of the lattice. (Phase transitions in the concentrated hydrides can sometimes be described in terms of this distortion exceeding the elastic limit. Overscreening can occasionally result in a local contraction.) The lattice relaxation results in a lowering of the interstitial potential at the muon or proton site, favouring localisation. Muons and protons are said to *self-trap* in this manner. The whole entity, *i.e.* interstitial particle plus screening charge plus elastic distortion, is referred to as a *small polaron*, illustrated in Figure 8. Erudite works refer to the particle " dressed" with electron and phonon clouds.

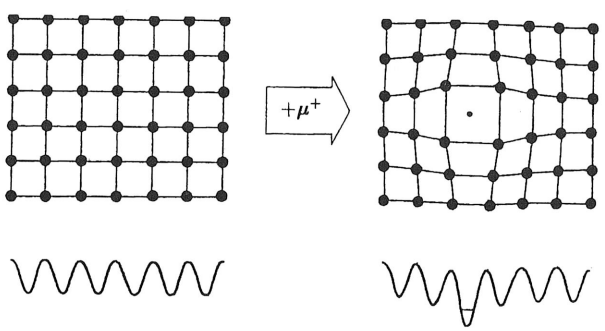

Figure 8. *The small polaron state of interstitial muons and protons, illustrating the local distortion of the lattice and self-trapping by lowering the interstitial potential.*

1.5.3 Quantum diffusion

The localisation or self-trapping does not imply that the small polaron state is necessarily immobile. In many metals, interstitial muons and protons diffuse with remarkable rapidity. μSR and other studies have been concerned with understanding the nature of the elemental step, *i.e.* the mechanism by which the small polaron can move between adjacent sites (given that the interstitial particle has to drag its screening charge and

local elastic distortion with it). The motion is not expected to be identical for muons and protons, though the comparison of their mobility may be valuable, with the muon more likely to exhibit *quantum diffusion.* By virtue of its greater zero-point energy in the interstitial well, the muon is often able to tunnel through the intervening barrier to the next site more readily than the proton (Roduner, this volume). In just a few cases – in certain insulators and semiconductors at low temperatures – the muonium tunnelling may be coherent, *i.e.* wave-like. More often it is incoherent, *i.e.* particle-like, meaning that the coherence length of the muon wavefunction is shorter than the elemental step-length: the particle, or rather the polaron, then moves step by step in a random walk. Quantum diffusion of muons in metals is dominated at low temperatures by the behaviour of the screening charge, which proves to be remarkably sluggish, hindering the muon's motion from one site to the next! (Although the Born–Oppenheimer approximation is usually assumed to hold, allowing a separation of muon and electron wavefunctions in muonated molecules (McKenna and Webster, 1985), this example of non-adiabaticity in metals is one observable instance of its breakdown.)

1.6 Conclusion

1.6.1 Ionic vs covalent bonding; diamagnetic vs paramagnetic states

In summary, the muon does not remain as a bare particle when implanted and thermalised in matter, but enters into chemical association with the host. An ionic description can sometimes be used; in metals this implies an associated screening charge; in non-metals purely electrostatic considerations are modified by varying degrees of covalency and consequent directional bonding. Muonium can exist as an interstitial atom or react to become covalently bound in molecular species.

In diamagnetic metals and in closed-shell molecular species, the muon spin rotation or resonance spectrum displays a single line, displaced from the Larmor frequency by a small Knight shift (metals) or chemical shift (molecules) and broadened by any nuclear dipolar interaction. Site assignments are usually possible from the orientation dependence of these features. More information is available on local electronic structure when the muon has quadrupolar neighbours, *via* level crossing resonance.

When the wavefunction of unpaired or spin-polarised electrons has some density at the muon site, large hyperfine fields can add or subtract to the external or distant-dipole fields which the muon experiences. Characteristic multiple frequencies appear in the μSR spectra when the electron spin states are long lived; an average paramagnetic shift results when they fluctuate rapidly, or when an ensemble or succession of conduction electrons is involved.

Atomic muonium is itself paramagnetic, as are the open-shell molecules or radicals formed by muonium addition to unsaturated organic compounds. In the trapped-atom state of muonium, the electronic wavefunction is centred on the muon but subject to some mixing with neighbouring atomic orbitals. In the molecular radicals (Roduner, this volume), major spin density is located on a nearby atom or atoms, rather than on the muon itself. The isotropic component of the hyperfine tensor provides a measure of the spin density on the muon, the anisotropic component the dipolar interaction. Spin densities on the other dipolar nuclei can be determined *via* hyperfine level crossing resonance.

1.6.2 Carbon from soot to diamond

Muon states in the different allotropes of carbon illustrate most of these possibilities. In graphite, which is commonly used as a standard of asymmetry in μSR experiments to calibrate polarisation, all implanted muons reach a diamagnetic state. A large and anisotropic Knight shift of the muon Larmor frequency reflects the almost 2D character of the electronic conduction in this material but still the screening is sufficiently effective to preclude muonium formation. In the fullerenes, muonium is formed and can exist as a trapped atom state, insulated by some potential barrier against reaction from *within* the cage. Muonium formed *outside* or in-between the bucky-ball cages, on the other hand, reacts quickly by addition at a double bond to form a molecular radical, as it does in a great many other unsaturated organic compounds. In diamond, muonium likewise exists in two distinct paramagnetic states. One is again a metastable trapped-atom state, located at the centre of an interstitial cage. The other more akin to a molecular radical: the muonium can be said to have reacted with the diamond lattice to adopt the so-called bond-centre site. Analogous cage-centred and bond-centred states are found in silicon and germanium, which also have the diamond-type lattice.

2 Muonium states and dynamics as a model for hydrogen in semiconductors

2.1 Introduction

An atomistic picture of interstitial hydrogen in semiconductors involves, as it does for hydrogen impurity in other materials, determination of the lattice sites and configurations adopted and the mechanisms of diffusion. An additional dimension is added in semiconductors, namely the possibility of different charge states of the defect centre – positive, neutral and negative – respectively the diamagnetic proton, paramagnetic hydrogen atom and diamagnetic hydride ion. μSR studies have been successful in examining the muonium counterparts of all these states, determining their local structure, their different stabilities, mobilities and interactions with charge carriers.

The interest in these studies stems from the realisation that, even as a trace impurity, hydrogen can have a profound effect on the electronic properties of semiconductors. The major and best known effect is the passivation of other impurities or defects, whereby hydrogen forms chemical complexes with them, removing their electrically active levels from the energy gap. This is illustrated in Figure 9. In crystalline semiconductors this effect is usually unwanted and harmful, since it destroys the electronic function of deliberate dopants, either donors or acceptors. In amorphous semiconductors, on the other hand, the saturation of the so-called dangling bonds, unpaired electrons at under-coordinated atoms in the random network, is beneficial; in fact, hydrogenation is essential for the production of electronics-grade material. (The concentration of hydrogen in hydrogenated amorphous silicon, for example, can be quite high – up to 20 at.% This is much more than is strictly necessary to passivate the dangling bonds.)

In addition, interstitial hydrogen displays an electrical activity of its own. One or two electrons can be captured and localised in defect levels within the semiconducting

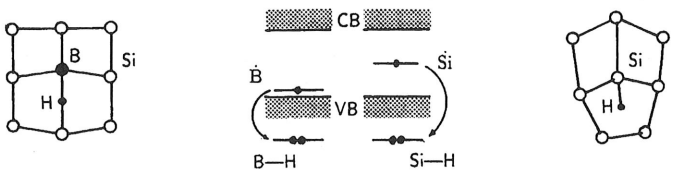

Figure 9. *Passivation of boron in silicon, replacing the acceptor level with a doubly occupied level in the valence band, and saturation of dangling bonds in a–Si, likewise removing mid-gap levels.*

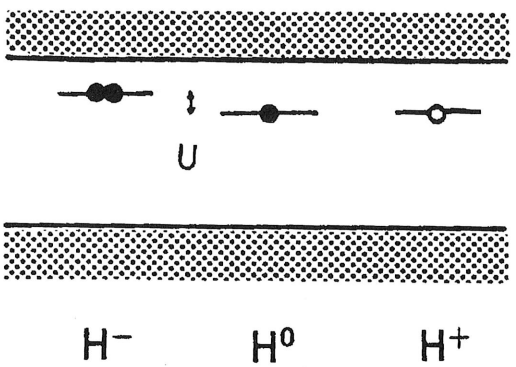

Figure 10. *Localised-state energy levels within the conduction-valence band-gap representing the hydride ion when doubly occupied, the interstitial hydrogen atom when singly occupied (and the interstitial proton when unoccupied.) A precise definition of the donor and acceptor levels, and of the Coulomb repulsion energy U, is given in Section 4 below.*

energy gap, or released from them, as illustrated in a simple fashion in Figure 10. This has been recognised only recently and μSR is currently providing unique information on how muonium, and by inference hydrogen, can act as a deep-level donor, acceptor or recombination centre, depending on the material and on the particular lattice site adopted. The studies rely on the supposition that the solid state chemistry of muonium and protium are sufficiently similar that the same crystallographic sites are preferred and, with due regard for differences in zero-point energy, the local lattice relaxations and electronic structures are essentially identical. More careful attention must be paid to the large isotopic mass ratio when it comes to interpreting interstitial diffusion rates; even here muonium may provide a reasonable model for hydrogen, however, when mobility is controlled by lattice distortions or carrier interactions (charge-state changes) rather than isotopic mass.

These notes are based on short review articles by Cox (1995) and Cox and Lichti (1997); they summarise what is now known about muonium centres in the elemental semiconductors Si and Ge and in compound semiconductors such as GaAs and InP and

explain how this information has been obtained from μSR spectra and muon spin dynamics. Many of the spectroscopic studies are classics of the early μSR literature, which has been reviewed thoroughly by Patterson (1988) but the dynamical studies concerning the interaction with charge carriers (generated thermally, optically or by doping) are more recent and ongoing. They reveal a quite unanticipated interplay between crystallographic site and charge state as well as very different mobilities for the different states; they show that under certain conditions, the diffusion of hydrogen in semiconductors may be controlled by charge-state transitions coupled to local configurational changes.

2.2 Neutral paramagnetic states: an example of metastability

In contrast to the situation in metals, the density of mobile conduction electrons in semiconductors is always insufficient to screen a defect charge. A positive muon can therefore bind a single unpaired electron to form atomic muonium, which represents a neutral paramagnetic centre. Such centres may be recognised *via* characteristic frequencies in the *muon spin rotation* spectra. The manner in which hyperfine constants or tensors are determined from these frequencies is described in detail in the literature (Patterson, 1988) and summarised in these lectures: see also Roduner (this volume).

Early μSR experiments made the surprising and important discovery that muonium centres are formed in two distinct paramagnetic states, which coexist at low temperatures in Si, Ge, GaAs and GaP. The original low-field spectrum for Si, compared with that for SiO_2, is shown in Figure 11. Note the different splittings of the lines marked Mu and the absence, in quartz, of those marked Mu*.

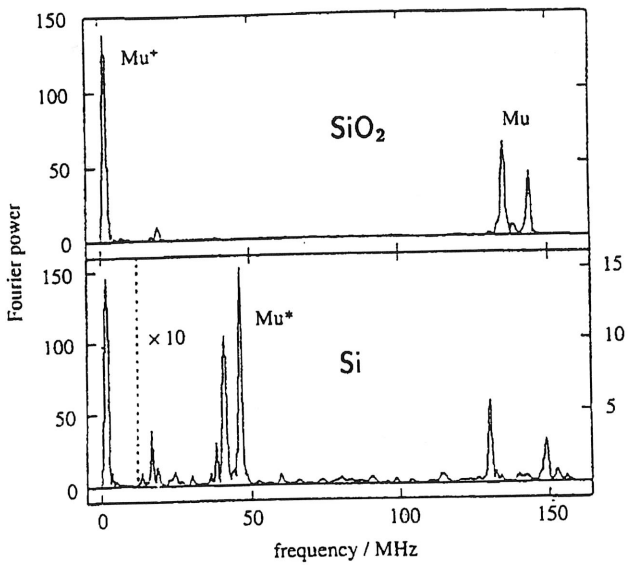

Figure 11. *μSR spectra for silica and silicon, recorded in the same low field (Brewer et al, 1973).*

A later spectrum for GaAs is shown in Figure 12, recorded in high field to avoid broadening or splitting of the lines due to nuclear couplings. (Nuclear moments are significant for both Ga and As, whereas the abundant isotopes of Si and Ge have none.) It also shows two distinct sets of lines, to be interpreted in terms of hyperfine parameters and site assignments, as follows.

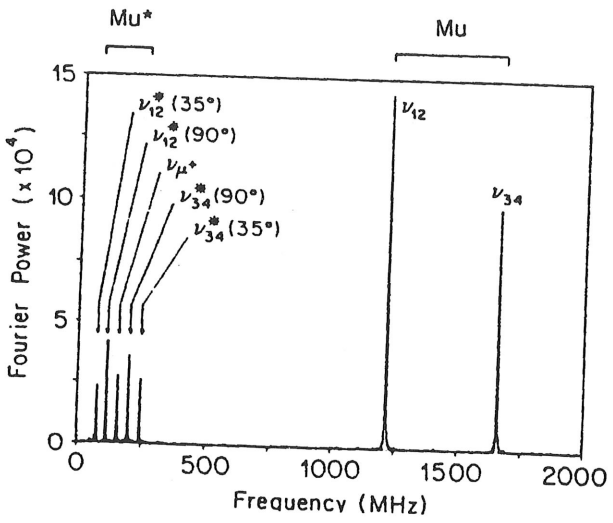

Figure 12. *High-field μSR spectrum of GaAs (Kiefl et al. 1985).*

2.3 The isotropic centres

In the spectrum for each material, the two lines marked Mu remain at the same frequencies however the (single crystal) samples are oriented in the magnetic field. They are also visible in powder spectra. The muonium centre responsible is therefore isotropic, with a scalar-product hyperfine interaction $A\mathbf{I}\cdot\mathbf{S}$ characterised by a single hyperfine parameter or "constant" A. Hyperfine constants are invariably given in units of frequency in the μSR literature; that for muonium is quartz is close to the vacuum-state value: $A = 4.46$GHz. In low-field spectra the splitting between the two lines is inversely proportional to hyperfine constant so the greater splitting in Si indicates a substantial (more than 50%) reduction in the semiconductor. High-field spectra give hyperfine constants more directly as the sum of the two frequencies (so that for GaAs is about 65% of the vacuum-state value). Other solids show varying degrees of reduction: precise values for the semiconductors are listed by Patterson (1988).

Originally known as "normal muonium", the isotropy of these centres in Si, Ge, GaAs *etc*, suggests location at the so-called T-site depicted in Figure 13. This is the only interstitial site in the diamond-type lattice with the necessary cubic symmetry. In fact this state is highly mobile so it is just possible that the instantaneous site is of lower symmetry, *e.g.* the antibonding site, and that any anisotropy of the hyperfine coupling is averaged to zero by the diffusion.

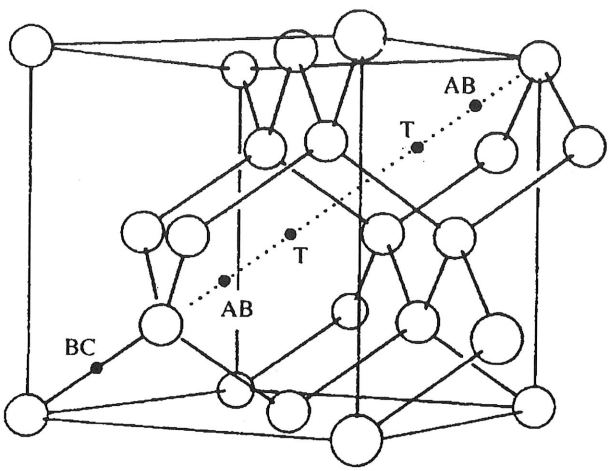

Figure 13. *The tetrahedrally coordinated or diamond-type lattice showing the cage-centre (T), bond-centre (BC) and antibonding (AB) sites. In the III–V compound semiconductors with the zinc-blende structure there are two inequivalent T-sites, with group-III or group-V atoms as nearest neighbours.*

2.4 The anisotropic centres

The groups of lines at low frequency, labelled Mu* in Figures 11 and 12, indicate the existence of a second paramagnetic state with much lower and highly anisotropic hyperfine coupling. The angular dependence revealed a centre with axial symmetry about the ⟨111⟩ or bond direction. Originally known as "anomalous muonium", it remained a puzzle for many years until separation of the hyperfine parameters into contact and dipolar terms (Equations 9–12) determined the muon site to be squeezed into an intrinsic bond, *e.g.* an Si–Si or a Ga–As bond, at or near its centre! Both muonium states carry a magnetic moment of one Bohr magneton but whereas the isotropic cage-centred state has major spin density centred on the muon (as expected for a "trapped atom") the anisotropic bond-centred state has most of it divided between two neighbouring host atoms. Sketched in Figure 14, only this site and structure explains how the electron can be so close to the muon without overlapping onto it, *i.e.* how the dipolar interaction can be so high while the contact interaction is so low: the muon lies at or near a node of the unpaired electron wavefunction (Cox and Symons, 1986). Level-crossing resonance has confirmed the model by measuring the partition of spin density on the neighbouring atoms (Kiefl *et al.* 1988).

2.4.1 Metastability, nomenclature

Now that the sites are known, we denote the isotropic state Mu^0_T (to distinguish it from free Mu) and the anisotropic state Mu^0_{BC} (instead of Mu*). The superscript indicates the charge state and the subscripts the crystallographic sites, as in Figure 13. Mu^0_T creates rather little local distortion of the tetrahedral cage whereas an intrinsic bond must be stretched by about 40% to accommodate Mu^0_{BC}; this difference in lattice relaxations

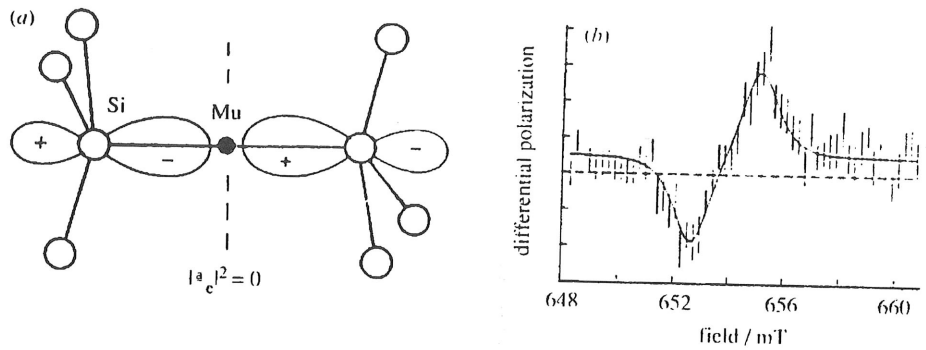

Figure 14. *The bond centre model for Mu* (Mu_T^0), showing the singly occupied orbital derived from the Si–Si antibonding orbital (Cox and Symons, 1986)) and the level crossing resonance with nearest neighbour ^{29}Si nuclei (Kiefl et al. 1988).*

accounts for the very different mobilities of the two states (Section 2.6).

The coexistence of Mu_T^0 and Mu_{BC}^0 is a remarkable example of *metastability*. Prior to the μSR studies, no isolated hydrogen defect centre was known and the bond-centred state was quite unanticipated. By implication, there should be not one but two distinct singly occupied defect levels denoted H^0 in Figure 10. In experimental and theoretical work prompted by the μSR findings, H_{BC}^0 has since been detected in ESR spectra and *ab initio* calculations which allow for lattice relaxation have found that it is the ground state of interstitial hydrogen in Si. The energy difference between the two sites proves to be rather small, however, so it may be that H_T^0 is the ground-state in other materials. H_T^0 has still not been detected by ESR; it must encounter and trap at other defects or impurites too quickly for this technique.

2.4.2 Amorphous semiconductors: repolarisation

In amorphous semiconductors, any distribution of hyperfine parameters in the random network is likely to broaden muon spin rotation spectra beyond detection – especially for the anisotropic centres. An indication of their existence can nonetheless be obtained from simple longitudinal-field measurements of the muon polarisation which remains after mixing of the muon-electron spin states by the hyperfine coupling. The variation with applied field, variously known as the *repolarisation*, *decoupling* or *quenching* curve, gives quite distinct signatures for the isotropic and anisotropic centres. These are illustrated in Figure 15: the isotropic state has a monotonic repolarisation curve but the signature of the bond-centred state is a striking cusp (Meier, 1994). (This cusp is analogous to the $\Delta M = 1$ level crossing resonances seen for muonium-substituted organic radicals in solids (Roduner, this volume) but for Mu_T^0 in semiconductors it appears at unusually low fields thanks to the low contact interactions.) Appropriate mixtures of the two contributions are recognisable in the experimental curves, both for polycrystalline and amorphous silicon (Cooke *et al.* 1994; Davis *et al.* 1995). This manner of detecting and characterising anisotropic centres in *disordered material* is remarkable – and unique to μSR.

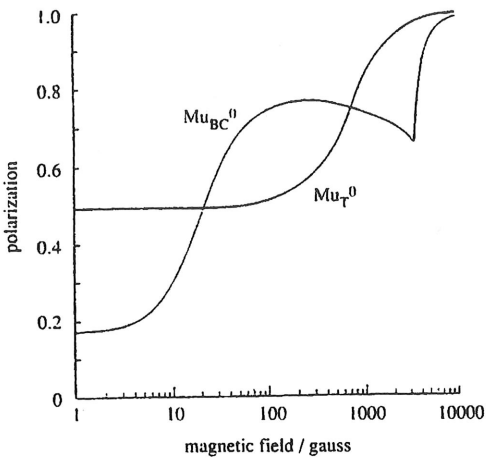

Figure 15. *Repolarisation curves computed for polycrystalline Si (Davis et al. 1994)*

2.5 Diamagnetic states

2.5.1 The charged centres: an example of bistability

For the ionic states, the site preferences are much more pronounced (Van der Walle *et al.* 1989; Briddon and Jones, 1990). In the elemental semiconductors Si and Ge, the positively charged defect should be located at the bond centre, denoted Mu_{BC}^{+}. That is, the interstitial muon (or proton) seeks out the region of high electron density provided by the spin-paired valence electrons. The negatively charged centre ($Mu^{-} = \mu^{+}e^{-}e^{-}$, analogous to the hydride ion) cannot exist in this location but is repelled to the cage-centre, denoted Mu_{T}^{-}. This dependence of site on charge state is a fine example of *bistability* in a defect centre.

The paramagnetic muonium centres correspond to singly-occupied energy levels within the forbidden gap between valence and conduction band (as in Figure 10). Lowering the Fermi energy by heavy p–type doping therefore favours ionisation of the neutral centres, creating Mu_{BC}^{+}, while raising it by heavy n–type doping favours double occupation, *i.e.* capture of a second electron to create Mu_{T}^{-}. Figure 16 confirms the existence of this latter state in GaAs by *level crossing resonance*, exploiting the presence of quadrupolar nuclei; this spectrum provides the strongest evidence for hydride ions in semiconductors. A similar identification of Mu_{BC}^{+} in p–type material is a high priority for the immediate future.

2.5.2 Passivation complexes

Although Si has no quadrupolar (and very few dipolar) nuclei, its common acceptor dopants B and Al do. This should permit observation of B–Mu and Al–Mu pairs *via* level crossing resonance. Simulated spectra are shown in Figure 17 – their detection would allow confirmation of the calculated electronic structure *via* measurement of the electric

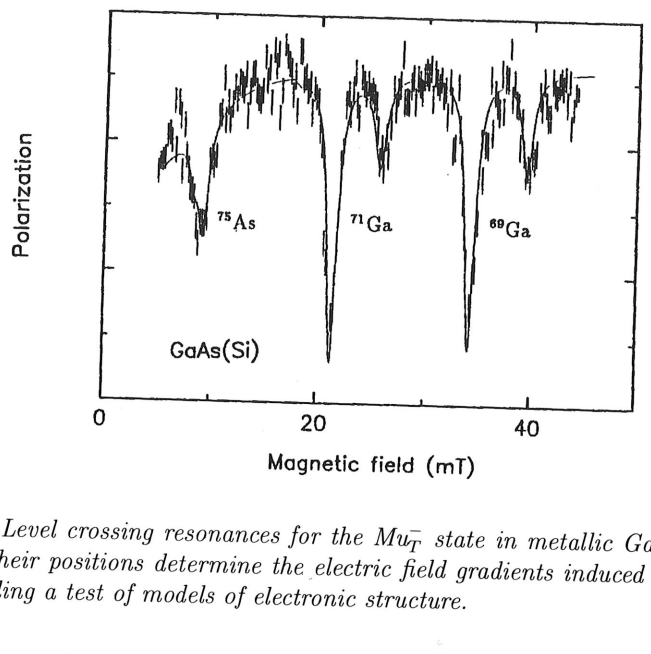

Figure 16. *Level crossing resonances for the Mu_T^- state in metallic GaAs:Si (Chow et al. 1995). Their positions determine the electric field gradients induced at neighbouring nuclei, providing a test of models of electronic structure.*

field gradients at the B and Al nuclei. Despite some careful searches, no convincing resonances have yet been reported. Either the muon does not have time to reach and pair with an acceptor within its lifetime (although see Section 2.6) or else it moves rapidly between the four bond-centre sites surrounding the subsitituent atom (thereby washing out the resonance). To date, the impact of μSR spectroscopy has been in characterising the isolated centres.

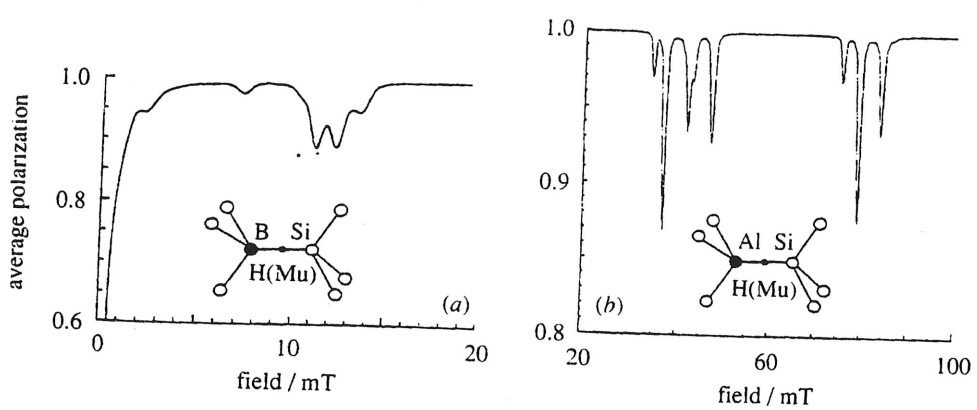

Figure 17. *Simulated level crossing resonances for (a) the B–Mu and (b) the Al–Mu pairs in p-type (Maric et al. 1990; Meier et al. 1994).*

2.6 Energy level schemes

Figure 18 summarises the site and stability information for both the neutral and charged centres. It uses two different energy level schemes of the types commonly used for deep-level centres, and gives the the correspondence between the two representations (Lichti, 1995; Cox, 1995). The configuration coordinate diagram emphasises the metastability for the neutral and the bistability for the charged centres; it shows the energy-level separations used to construct donor and acceptor levels within the semiconducting gap. The donor state is defined as usual to be neutral when occupied, positive when empty. So its position is set by the ionisation energy denoted $E_{\rm BC}^{0/+}$. For this type of *amphoteric centre*, (a deep-level centre which can act as both donor and acceptor), the acceptor level is defined to be negative when doubly occupied, neutral when singly occupied. Normally a doubly occupied level lies higher than a singly occupied one by the Coulomb repulsion or correlation energy U (as in the simpler representation of Figure 10) but the order can be inverted when a site change or lattice distortion is involved: in the notation of Figure 18, $U = E_{\rm BC}^{0/+} - E_{T/BC}^{-/0}$.

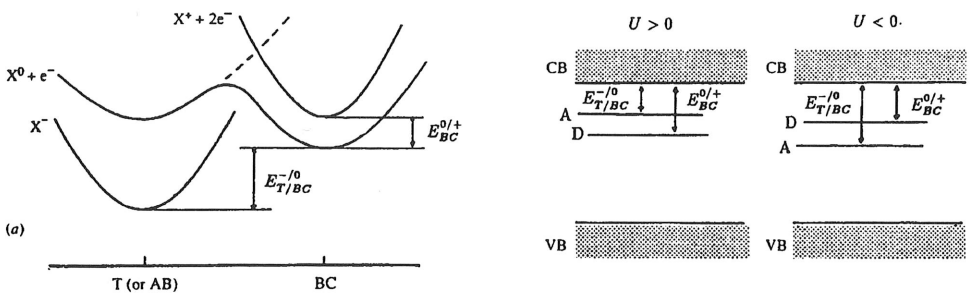

Figure 18. *The configuration coordinate diagram (a) for hydrogen or muonium centres (X=H, Mu) and the corresponding deep donor and acceptor levels (b). The acceptor level A lies higher in the gap than the donor level for positive U, lower for negative.*

Whether hydrogen is a "negative-U centre" in silicon is a question of current debate, which μSR measurements may help resolve. Figure 18 should be essentially the same for H and Mu; they will have significantly different zero-point energies within each potential well, although the isotope effects in the donor and acceptor levels are expected to be small. If U is positive, the three states $H_{\rm BC}^{+}$, $H_{\rm BC}^{0}$ and H_{T}^{-} should be stabilised in turn, as the Fermi level is moved upwards through the gap by doping. If it is negative, there is no position of the Fermi level for which singly occupied levels are stable. In either case, observation of $Mu_{\rm BC}^{0}$ and Mu_{T}^{0} together in μSR spectra implies that thermodynamic equilibrium is not achieved on the timescale of muon lifetime.

2.7 Charge-state and site transitions

The neutral muonium centres Mu^0_{BC} and Mu^0_T are observed at low temperature in pure or lightly doped material. On heating, they convert to diamagnetic Mu^+_{BC} by ionisation, *i.e.* by loss of the unpaired electron to the conduction band. In Si, the one-way reaction

$$Mu^0_{BC} \rightarrow Mu^+_{BC} \tag{24}$$

sets in just above 100K and the one-way reaction

$$Mu^0_T \rightarrow Mu^+_{BC} \tag{25}$$

around room temperature. (This latter involves a change of both site and charge state, presumably in that order.) In the region where the ionisations are slow, RF resonance is invaluable in displaying the final diamagnetic state (Kreitzman *et al.* 1995). When they are fast, full asymmetry is recovered in the muon spin rotation spectrum at the Larmor frequency. On further heating, or on illumination, a remarkable depolarisation or *relaxation* sets in, as illustrated in Figure 19. This is visible in both longitudinal and transverse field.

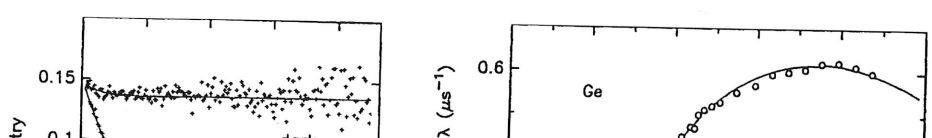

Figure 19. *Muon depolarisation in Si, with and without illumination by a Xe flashlamp, and the temperature dependences of the thermally induced depolarisation rates in Ge (Cox and Lichti, 1997; Lichti et al. 1994).*

The high-temperature relaxation is due to trapping and detrapping of the thermally generated conduction electrons by the muon, *i.e.* repeated formation and ionisation of muonium. The variation of this relaxation rate with applied magnetic field determines the muon-electron hyperfine interaction and thereby identifies the active muonium state. The initial peak near room temperature for Ge is assigned to charge-state cycles at the bond-centre, expressed in Equation 26 (this is the two-way version of reaction 24). The broader feature is assigned to coupled charge and site transitions, with Mu^0 at the cage-centre, as in Equation 27 (this is the two-way version of reaction 25: Lichti *et al.* 1996, 1997).

$$Mu^0_{BC} \overset{\pm e}{\longleftrightarrow} Mu^+_{BC} \tag{26}$$

$$Mu^0_T \overset{\pm e}{\longleftrightarrow} Mu^+_{BC} \tag{27}$$

Only cycle 27 shows up in muon relaxation in hot Si (Chow *et al.* 1993). Yet another cycle dominates in n–type GaAs, namely the successive capture of electrons and holes,

expressed in Equation 28 (Lichti *et al.* 1994; Chow *et al.* 1996). By implication, cage-centred hydrogen acts as a recombination centre in this material.

$$\mathrm{Mu_T^-} \overset{+h,+e}{\longleftrightarrow} \mathrm{Mu_T^0}. \tag{28}$$

These processes have become known as "charge exchange", distinguishing them from the mechanism of muonium depolarisation which occurs in highly doped material, namely "spin exchange". (A description of the depolarisation in terms of alternating or intermittent hyperfine coupling is given in Section 3.) Optically induced relaxation is observable at all temperatures, affecting also the neutral centres at low temperature (Iwanowski *et al.* 1994; Kadono *et al.* 1994, 1997; Scheuermann, 1997). The exact nature of the interaction with photo-generated carriers has in most cases still to be clarified, *e.g.* to distinguish spin and charge exchange from any direct photostructural transitions. Such experiments should establish whether hydrogen impurity influences photoconductivity or other opto-electronic functions.

2.8 Diffusion and trapping

In the tetrahedrally coordinated semiconductors, $\mathrm{Mu_T^0}$ is highly mobile at all temperatures (Patterson, 1988). Measurements for GaAs are shown in Figure 20; the remarkable minimum in mobility around 90K in fact provided the first indication of *quantum diffusion* of the neutral muonium atom (Kadono, 1990). (The analysis of longitudinal-field relaxation data for hop-rates and the change from particle-like to wave-like motion are described in Section 3 and Storchak, this volume) The $\mathrm{Mu_{BC}^0}$ state is immobile in Si and GaAs, locked in place by the large local distortion. By implication, neutral hydrogen diffuses *only via* the tetrahedral cage sites. This may not be the case in other semiconductors: the energy barrier between the T and BC sites is low in Ge, for instance, and it seems likely that both sites are visited in the course of diffusion of the neutral state above about 50K (Lichti *et al.* 1997).

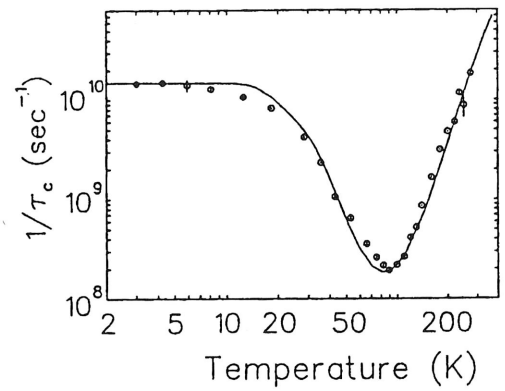

Figure 20. *Temperature dependences of mobility for Mu_T^0 in GaAs (Kadono et al. 1990).*

Figure 21(a) shows relaxation data for heavily doped n–type and p–type GaAs, favouring observation of $\mathrm{Mu_{BC}^+}$ and $\mathrm{Mu_T^-}$, respectively. The onset of motional narrowing occurs

around 200K for the positive centre but only at the higher temperature of 500K for the negative. A similar behaviour is found in InP, although in this more ionic material the positive ion can itself occupy two different sites – either the bond centre as usual or the cage centre defined by the more electro-negative Group-V ions (Lichti *et al.* 1997). Hop rates are shown in Figure 21(b). Given this difference in the mobilities of different charge states, and of different onset temperatures, it appears that the mechanism of hydrogen diffusion in semiconductors may vary considerably according to material, temperature and doping. In certain régimes it must involve a combination of charge states, controlled by carrier capture and loss.

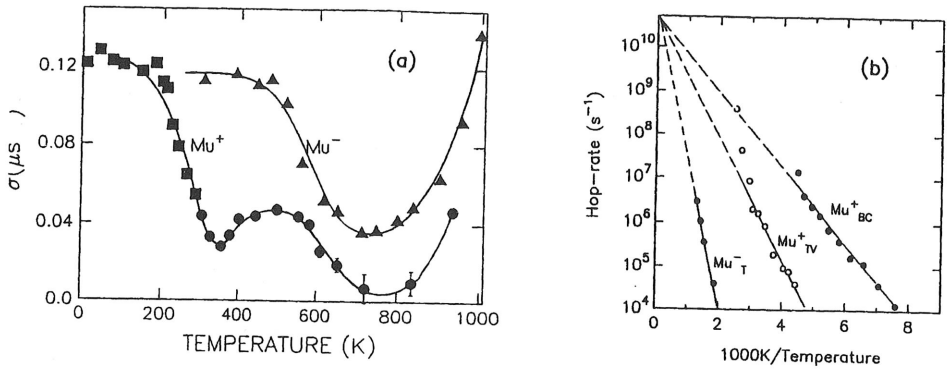

Figure 21. *Temperature dependences of TF–μSR Gaussian relaxation rates for n and p–type GaAs (Chow et al. 1997) and hop rates for the various charged centres in InP (Lichti et al. 1997).*

In p–type samples of both materials a trapping peak in the relaxation data is strongly suggestive of pairing with the acceptor atoms, at temperatures where the muon diffuses fast enough to seek these out. This is probably the best evidence for the elusive passivation complexes, described in the introduction.

2.9 Conclusions

Building on earlier spectroscopic studies, predominantly of the neutral muonium states, these more recent results imply a remarkable interplay between charge state and crystallographic location for hydrogen in semiconductors. This was quite unanticipated and carries two major implications for the functional properties of these materials. The first is that interstitial hydrogen can act as a centre for electron trapping and detrapping, or electron-hole recombination. The second is that the elusive *transport state* of hydrogen in semiconductors is not one but several states. It switches from the positive ion (the proton) to the neutral interstitial atom to the negative (hydride) ion, according to temperature and to the type and level of doping. In pure or lightly doped material at high temperatures it seems likely that diffusion is controlled by changes of site and lattice configuration, coupled to charge-state transitions. In other words, diffusion is linked to the interaction with charge carriers. Work on Si has reached the stage where all these properties of the isolated states can be accounted for in terms of a reasonably consistent

set of energy levels and barriers. Future work is aimed at obtaining similarly complete sets of parameters for each material of importance and checking that these also account for the response to illumination. A more detailed understanding of the pairing with dopant atoms remains to be achieved; here a spectroscopic determination of the local electronic structure of the passivation complexes would be another major scoop for μSR!

3 Spin-lattice relaxation

3.1 Introduction

On implantation into a sample, muons thermalise rapidly. At least, they lose their excess kinetic energy and find a minimum of electrostatic potential energy in a time which is short compared with their lifetime and usually over before data dating begins. A μSR experiment then displays the evolution of spin polarisation on a microsecond timescale. This implies that the muons' spin degrees of freedom come to equilibrium with the environment only much more slowly than kinetic thermalisation, if at all. In fact, they may never reach the sample temperature (in solids, the lattice temperature) before the muons decay but their tendency to do so is known as *spin-lattice relaxation.*

A source of confusion in the μSR literature, as in conventional magnetic resonance, is that the term "relaxation" covers too many different processes. For instance, there is cross-relaxation, which is the exchange of polarisation with neighbouring spins, nuclear or electronic; it is observed in zero-field, in very weak longitudinal fields, or under conditions of level-crossing resonance (Uemura, this volume). Then there is so-called spin-spin relaxation, which represents the damping of the muon spin rotation signal in a transverse field, when this is due to dipolar interactions with the host spins (De Renzi, this volume). Since the muons are always probe spins, interacting with the host spins but not with each other, the term *spin-spin relaxation* does not have exactly the same meaning in μSR as it does in NMR, where it establishes a common spin temperature for a homonuclear spin system. Spin-spin and cross relaxation are due to time-independent spin-spin interactions and give information on muon sites and local structure as long as the muon is static, or nearly so.

Spin-lattice relaxation, when it occurs on a measurable timescale, gives dynamical rather than structural information. It is caused by thermally excited fluctuations of the muons' magnetic environment, *e.g.* by the intrinsic fluctuations of the host spins in magnetic materials or by the motion of the muons themselves. That is, it occurs when the spin-spin interactions are time dependent: it modifies the effects of spin-spin or cross relaxation and can wash out spectroscopic and structural information if it is too fast. It leads to an irreversible, *i.e.* irrecoverable, loss of polarisation. On the other hand, spin-lattice relaxation data can usually be interpreted in terms of the relevant motional correlation times whether or not the muon site and precise chemical state are known.

Spin-lattice relaxation is well understood in conventional magnetic resonance, and there are particular similarities between the muon response and the response of other spin-$\frac{1}{2}$ nuclei, notably protons. Thorough descriptions are to be found in the standard NMR textbooks, therefore, *e.g.* Abragam (1961), Slichter (1963, 1990) and many others. The main features for spin-$\frac{1}{2}$ particles, represented by a two-level system, are summarised

and adapted to the case of muons in Sections 3.2–3.4, below. The principal differences with protons and other nuclei are the high starting polarisation and the unique dynamic range determined by the muon lifetime and detection techniques. (The high starting point is almost unprecedented in NMR except when dynamic nuclear polarisation is employed.) This range is rather narrow but is suited to much faster relaxation than conventional NMR and corresponds to useful and sometimes unique windows on motional correlation times. It also means that, in high magnetic fields, longitudinal muon relaxation is only significant if electronic moments are involved.

A major application of muon spin-lattice relaxation measurements is to the study of spin-correlations and fluctuations in magnetic materials: this is merely introduced in this section, aspects specific to different classes of magnetic material being dealt with by others (Brewer, this volume). Some less common (*i.e.* non-exponential) relaxation functions and unusual mechanisms (*e.g.* intermittent hyperfine coupling, including spin and charge exchange) are mentioned in Section 3.5. The remaining major application is to the study of muonium diffusion and the molecular dynamics of muonated radicals; here we are concerned with hyperfine coupling to an individual electron whose own spin states may be relatively long-lived. Some ESR analogies are valuable (see *e.g.* Atherton, 1993) but the ability of μSR to make field-scans of relaxation rate, *i.e.* to explore its variation over a much wider range of magnetic field than is possible for ESR without the necessity of retuning spectrometers or resorting to field-cycling, has shown up some new features. This area has had to be developed specifically for μSR. At low fields or in the vicinity of level-crossing resonances the coupling of the muon and electronic spin states requires a description in terms of four or more energy levels instead of two. This is dealt with at some length in Section 3.6. It leads to simulations of the field and temperature dependence of relaxation rate which are illustrated by literature data for C_{60} and related to observations of level crossing resonance by *integral counting* techniques.

3.2 Spin states, energy levels and polarisation

Being a spin–$\frac{1}{2}$ particle, a muon's magnetic energy is quantised in a magnetic field into two levels. These split apart linearly with the field strength B as in Figure 22, according to two equivalent expressions:

$$\delta E = g_\mu \beta_n B \tag{29}$$

$$\delta E = \hbar \gamma_\mu B. \tag{30}$$

This is called the Zeeman energy. In version (29), the muon g-factor, like that of the electron, is closely equal to 2 (Jungmann, this volume); β_n is the nuclear magneton. Version (30) is the more commonly used form, involving the the muon gyromagnetic (sometimes magnetogyric!) ratio. This is

$$\gamma_\mu \approx 2\pi \times 13.6\text{kHz/G}. \tag{31}$$

It is specific to the muon and, for comparison, is 3.18 times the proton value. (It is larger, therefore, than that for all other nuclei – a fact which is important for level crossing resonance.) Nonetheless these energies are small by any standards: for illustration, the muon Zeeman splitting in 10kG (*i.e.* 1T) is $\delta E \sim 10^{-25}$joule, equivalent to about 0.5μeV or 6mK.

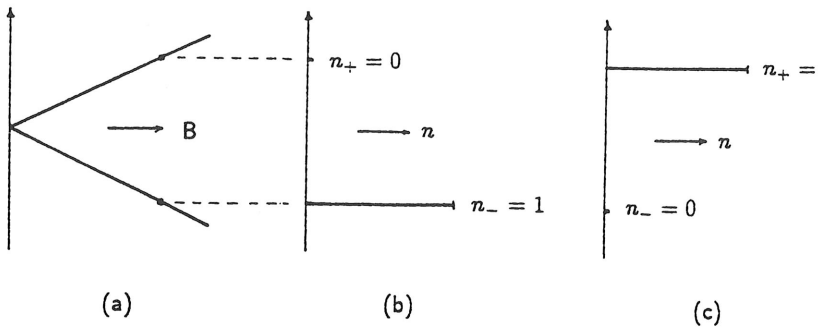

Figure 22. *Muon Zeeman energy (a) and occupancies of the levels at a given longitudinal field for $P = +1$ (b) and $P = -1$ (c).*

The corresponding eigenstates are affectionately known as *spin-down* (the ground state, with energy $-\frac{1}{2}\hbar\gamma_\mu B$) and *spin-up* (the metastable state, with energy $+\frac{1}{2}\hbar\gamma_\mu B$), referring to the two possible projections of the muon's intrinsic angular momentum onto the field direction. The most explicit notation for the two states is $|I, I_z\rangle = |\frac{1}{2}, -\frac{1}{2}\rangle$, $|\frac{1}{2}, +\frac{1}{2}\rangle$, but the abbreviations $|-\rangle$, $|+\rangle$ or other notations such as ψ_-, ψ_+ or $\psi_\uparrow$, $\psi_\downarrow$ or (especially in the chemical literature) ψ_α, ψ_β are common. Since the spin eigenstates (unlike the spatial wavefunctions) are not continuous functions of any known coordinate, any two symbols will do. Use whatever is convenient!

In 4MeV "surface muon" beams, the muons are prepared in a unique spin state (Eaton, this volume). That is, they are all spin-up in a longitudinal field applied parallel to the beam momentum or all spin-down in a field applied antiparallel. Their polarisation is said to be 100% on entry into the sample: $P = \pm 1$. Figure 22(b,c) depicts these situations in terms of occupancies of the two energy levels. Clearly neither is a state of thermal equilibrium. In general, we expect partial occupation of both levels, in which case the polarisation is defined to be

$$P = \frac{n_- - n_+}{n_- + n_+}. \tag{32}$$

If the spin degrees of freedom were in thermal equilibrium with the sample (*i.e.* at the same temperature T as its lattice, usually[1]), the two occupancies would be related by the Boltzmann factor, as in Figure 23:

$$\frac{n_+}{n_-} = \exp\left(\frac{-\delta E}{k_B T}\right), \tag{33}$$

leading to

$$P_\infty = \tanh\left(\frac{\hbar\gamma_\mu B}{2k_B T}\right). \tag{34}$$

[1]Hence the phrase *spin-lattice*, or the alternative phrase, *spin-phonon* relaxation. In fact, the equilibrium is often with an electronic temperature, but it is rare in μSR for this to differ from that of the lattice or "phonon bath". The term *spin-lattice* relaxation is commonly used even in fluid phases! Here the appropriate temperature is that of translational, rotational or vibrational degrees of freedom, as we see in Section 3.6 below.

Now we can see that thermal equilibrium polarisation P_∞ is usually small, since muon Zeeman energy is usually so much smaller than thermal energy . Equation 34, which is the Brillouin function for spin-$\frac{1}{2}$ particles, may then be approximated as

$$P_\infty \approx \frac{\hbar\gamma_\mu B}{4k_B T}. \tag{35}$$

For instance, at room temperature ($k_B T = 25$meV) and at 10kG ($\delta E = \hbar\gamma_\mu B \approx 0.5\mu$eV), $P \approx 0.0005\%$! Even for B =10kG and T=100mK, expensive conditions already requiring a superconducting solenoid and a dilution refrigerator, we have only $P \approx 1.6\%$. For all but the most extreme sample environment conditions, therefore, thermal equilibrium polarisation is negligible compared with a starting polarisation of 100%. This is one reason, of course, why μSR is more sensitive *per spin* than conventional NMR, the other being the the manner in which μeV spin transitions are detected at MeV energies *via* the muon decay.

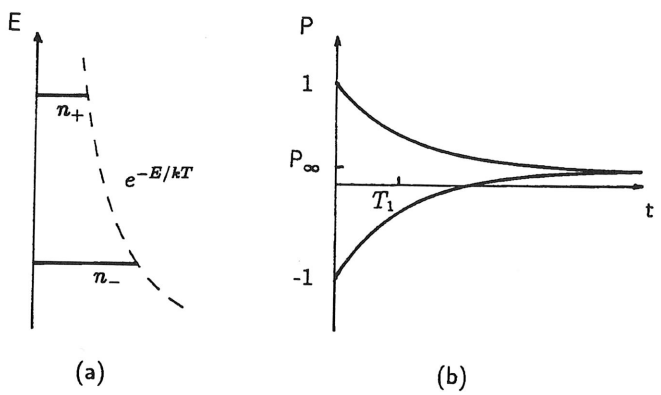

Figure 23. *Thermal equilibrium occupancies (a) of the two Zeeman levels in a longitudinal field (Equation 33) and spin-lattice relaxation (b) from the initial conditions of Figure 22(b,c) (according to Equations 37, 38 below).*

Over and above any spin-spin or cross relaxation, therefore, we expect that muon polarisation will evolve by spin-lattice relaxation inside the sample, tending to decrease or *relax* from its initial value close to 100% towards an equilibrium value close to zero. The question is whether there is any mechanism to achieve this on the timescale of the muon lifetime. Some perturbation is required which flips the muon spins, *i.e.* induces transitions between the spin-up and spin-down eigenstates. For the present description we stick to the simplest case of a high longitudinal field, well away from any resonance condition. (The effect on level crossing resonance is mentioned in Section 3.6.3.) We consider different possible mechanisms below but begin in Section 3 with some common features.

3.3 Rate equations and exponential relaxation

Assuming there are significant upward and downward transition probabilities, we can write rate equations for the occupancies of the two states (in an obvious notation):

$$\begin{aligned} \dot{n}_+ &= -W_\downarrow n_+ + W_\uparrow n_-, \\ \dot{n}_- &= W_\downarrow n_- - W_\uparrow n_-. \end{aligned} \tag{36}$$

which combine with Equation 32 to give[2]

$$\frac{d}{dt}\delta P = -(W_\uparrow + W_\downarrow)\delta P, \tag{37}$$

where $\delta P = P(t) - P_\infty$, the difference between the instantaneous and thermal-equilibrium polarisation. The solution is a simple exponential decay from the initial polarisation towards the thermal equilibrium value:

$$\begin{aligned} \delta P(t) &\propto e^{-(W_\uparrow + W_\downarrow)t} \\ &= e^{-\lambda t} \\ &= e^{(-t/T_1)}. \end{aligned} \tag{38}$$

Various notations are given here: the most common in μSR is to call the relaxation rate λ, equal to the sum of the upward and downward transition probabilities. A notation common in conventional magnetic resonance, and sometimes borrowed in μSR, is to define a *relaxation time*, $T_1 = \lambda^{-1}$. Notice that if the starting polarisation is negative, and the thermal equilibrium polarisation significant, there is a change of sign in the course of the relaxation, as in Figure 23(b). (This is common in NMR, following a 180° pulse, but rarely seen in μSR).

Although the thermal equilibrium polarisation is usually negligible in μSR compared with the high starting value, it is necessary to describe situations where the initial polarisation is less than 100%, or where some fraction shows no relaxation (*e.g.* of muons stopped outside the sample in a silver mask or holder). We then would write

$$P(t) = p_1 G_{\|}(t) + p_2, \tag{39}$$

or equivalently, in terms of the asymmetries or amplitudes of the μSR signals,

$$a(t) = a_1 G_{\|}(t) + a_2. \tag{40}$$

Here $G_{\|}(t)$ is called the *relaxation function*, defined so that $G_{\|}(0) = 1$; the subscript specifies that this is longitudinal relaxation, in line with the applied field (or, in the case of zero field, in line with the initial muon polarisation). Other common notations for longitudinal relaxation functions are $G_z(t)$ and $G_{zz}(t)$. In this simple case it is exponential; some other functional forms that are commonly encountered are introduced in Section 3.5. Somewhat surprisingly, the shape of the muon response or relaxation function does not depend on whether the longitudinal field is parallel or antiparallel to the beam.

[2]Exercise for the student! Total occupancy is conserved, so set $n_+ + n_- = 1$. Note that the upward and downward transition probabilities must be in the inverse Boltzmann ratio to ensure detailed balance at thermal equilibrium. Do not worry here about whether thermal equilibrium is reached within the muon lifetime: suppose $\tau_\mu = \infty$!

3.4 BPP relaxation: mechanisms, dynamic range

Spin-lattice relaxation requires some fluctuation of the muon's magnetic environment. If the field at each muon site were exactly parallel (or antiparallel) to the beam polarisation and perfectly "quiet", the muons would remain in one or other of the stationary states of Figure 22(b,c). A time-dependent perturbation of the local field is needed which

(a) has a component transverse to the main or static-average longitudinal field and

(b) can supply a quantum of energy equal to the Zeeman splitting, so as to flip the muon spins.

The first condition means that purely longitudinal fluctuations are ineffective – they modulate the Zeeman energy but do not induce transitions between the levels – the spin eigenstates are not a function of field strength. (This is only true for the 2-level system – it is quite otherwise for the 4-level system of muonium – see Section 3.6!) The second implies that the power spectrum of the fluctuations must contain significant intensity at the frequency corresponding to the Zeeman splitting, *i.e.* at the Larmor frequency:

$$\omega_\mu = \delta E/\hbar = \gamma_\mu B. \tag{41}$$

Note that it is common to work in terms of the angular frequency. Beware the factors of 2π arising from the definition of gyromagnetic ratio (Equation 31)! At 10kG, for example, $\nu = 136\text{MHz}$; $\omega = 8.5 \times 10^8$ radians/sec.

A common formulation of time-dependent perturbation theory is Fermi's Golden Rule, which for the present case gives

$$W \approx (\gamma_\mu B_l)^2 J(\omega_\mu); \tag{42}$$

here W is the transition probability between the two spin states, neglecting now the difference between upward and downward probabilities so that $\lambda = 2W$ (A more sophisticated treatment involving the initial and final phonon states of the lattice, as well as the spin states, gives the Boltzmann ratio for $W_\uparrow/W_\downarrow$ necessary for detailed balance at thermal equilibrium.) B_l in Equation 42 is the rms amplitude of transverse fluctuations of the local field and $J(\omega)$ is the spectral density function or power spectrum of the fluctuations. Spin-lattice relaxation samples this spectrum at $\omega = \omega_\mu$, *i.e.* at the muon Larmor frequency: Figure 24 illustrates how the power at this frequency can be small if the spectrum is too narrow (fluctuation slow) or too broad (fast), but goes through a maximum for a well matched fluctuation or hop rate. The effect is shown explicitly in Figure 25(a).

The usual form of the spectral density function is a simple Lorentzian, characterised by a single correlation time τ_c:

$$J(\omega) = \frac{\tau_c/\pi}{1 + \omega^2\tau_c^2}. \tag{43}$$

To within some numerical factor, the relaxation rate may then be written

$$\lambda = T_1^{-1} \sim (\gamma_\mu B_l)^2 \frac{\tau_c}{1 + \omega_\mu^2\tau_c^2}. \tag{44}$$

This is commonly known as the BPP expression, after its original formulators, Bloembergen, Purcell and Pound (1948). It is plotted as a function of the fluctuation rate $1/\tau_c$ in

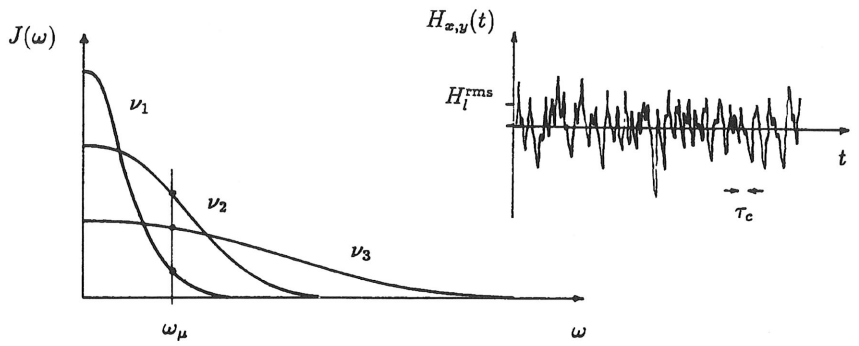

Figure 24. *Spectral density functions (Equation 43) for three values of the fluctuation rate $\nu = \tau_c^{-1}$ ($\nu_1 > \nu_2 > \nu_3$). The time-dependent fluctuations of the local field characterised by a correlation time τ_c are sketched in the insert.*

Figure 25(a) and of magnetic field in Figure 24(b). These are, so to speak, different 2D cuts through the spectral density function (Equations 43, 44). In diffusion problems, τ_c can usually be identified with the muon residence time, so that $1/\tau_c$ is the *hop rate*. Figure 25(a) illustrates the various the rate maxima, given by the condition that fluctuation rate matches the transition frequency:

$$\omega_\mu \tau_c = 1. \tag{45}$$

The magnetic resonance literature refers to these as "T_1-minima"; they provide an invaluable calibration for the *absolute value* of fluctuation rate.

Notice that relaxation rate is proportional to fluctuation rate in the slow fluctuation régime but *inversely proportional* to it for fast fluctuation. A relaxation rate which becomes slower as fluctuation rate increases seems somewhat counter-intuitive but this is actually the more common situation: it represents the fact that the muon spins cannot respond if the fluctuations become too fast (*i.e.* much faster than Larmor precession). Notice that the field dependence of relaxation rate (shown on log scales in Figure 25b) is a one-to-one map of the spectral density function (linear scales in Figure 24) and the "shoulder" where it begins to decrease provides a good estimate of the (inverse) correlation time, *via* Equation 43. The absence of a field dependence is likewise a good means of distinguishing a fast dynamic process from cross relaxation due to some static spin-spin interaction.

Also plotted in Figure 25(a) is the transverse field relaxation rate or *linewidth* of the muon spin rotation spectrum; this is denoted T_2^{-1}, as in conventional magnetic resonance (De Renzi, this volume). The plateau value at zero and small fluctuation rates is spin-spin, not spin-lattice relaxation: it represents depolarisation due to dephasing of the precession signal in the presence of a field distribution, *e.g.* due to dipolar coupling to neighbouring spins (De Renzi, this volume) or, in superconductors, inhomogeneous flux penetration (Lee, this volume). In this régime, $T_2^{-1} > T_1^{-1}$. (Note that a static field distribution causes no *longitudinal* relaxation.) Fluctuation causes a reduction of this depolarisation rate or

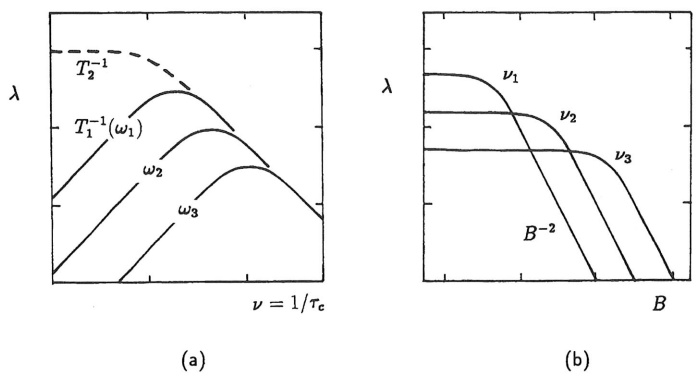

Figure 25. *Variation of BPP relaxation rate with (a) fluctuation rate, and (b) magnetic field. The scales are logarithmic, marked in decades.*

linewidth, commonly known as *motional narrowing.* (There is usually an accompanying change of lineshape in the muon spin rotation spectrum from Gaussian in the static limit to Lorentzian in the motionally narrowed régime (Uemura, this volume). Note also that since the muons are dilute probe spins, the NMR distinction between T_2 and $T_2{}^*$ does not usually apply.) In the fast-fluctuation régime ($\omega_\mu \tau_c \ll 1$), transverse and longitudinal relaxation rates become equal: $T_2^{-1} = T_1^{-1}$.

We now consider orders of magnitude for specific mechanisms.

3.4.1 Non-magnetic materials

By these we mean materials with nuclear, but not atomic, moments. We first make an order of magnitude estimate to see whether the fluctuation of local fields from nuclear dipole moments alone can cause measurable spin-lattice relaxation for muons. Consider Cu metal, for which the local fields and muon hop rates are known from transverse field μSR (Hartmann 1980). We have $B_l \approx 4$G and hop rates varying in the range $4 \times 10^4 < 1/\tau_c < 10^7 \mathrm{s}^{-1}$ below room temperature. The BPP expression then predicts,[3] for instance for a longitudinal field of $B = 1$kG, values spanning roughly

$$10^{-6} < \lambda < \times 10^{-4} \mu\mathrm{s}^{-1},$$

i.e.

$$1\mathrm{s} > T_1 > 100\mathrm{ms}\,!$$

These are relaxation rates or times which are typical of conventional NMR but which are *far too slow for μSR.* The same is true of relaxation caused by lattice vibrations of the Cu nuclei, rather than site-to-site motion of the muon. For this reason, simple metals are commonly used as a standard of polarisation with little or no longitudinal relaxation; only at weak longitudinal fields, $B \sim B_l$, does motional relaxation show up *via* the dynamic Kubo–Toyabe function. (Notice that the relaxation rate of the "1/3 tail" of this function

[3]Exercise for the student! Use Equation 44 and show that conditions remain in the slow fluctuation régime throughout, so that $\lambda \sim (B_l/B)^2.(1/\tau_c)$.

becomes equal to $\frac{2}{3}\frac{1}{\tau_c}$ for slow diffusion, giving a direct or absolute measurement of hop rate (Uemura, this volume). This contrasts with Equation 44, where hop rate can only be extracted if B_l is known.)

This estimate illustrates a general rule, namely that spin-lattice relaxation is unmeasurably slow for electronically diamagnetic muon states in high fields. For the case of muons in copper, and other simple metals, one can ask what is the effect of the conduction electrons, *i.e.* the Pauli paramagnetism. In principle, spin-flip scattering of the conduction electrons should depolarise the muons – this is the Korringa mechanism, which in NMR studies of metals is usually the dominant cause of nuclear relaxation (De Renzi, this volume). (It is not spin-lattice relaxation, strictly speaking, since the interaction is with electrons rather than with phonons, but the effect is the same.) The mechanism originates in the hyperfine interaction between the nuclei and the conduction electrons: the static average of the interaction gives rise to the Knight shift and the thermal modulation about this average causes the relaxation. The absolute values are still small by μSR standards and no clear examples yet exist in the μSR literature.

3.4.2 Magnetic materials

Moving from simple metals to metals where the conduction electron spins begin to correlate with each other, *e.g.* to the transition metals with itinerant moments (not to mention the more exotic forms of correlation in rare earth and actinide alloys), the Korringa mechanism takes on a new significance and can become a powerful mechanism of muon spin relaxation. Pronounced temperature dependences reflect the development of spin correlations. This is dealt with in other Lectures and exemplified by various classic μSR studies, *e.g.* of the itinerant magnet MnSi (Uemura, this volume) and of the onset of moment localisation in Mn alloys (Rainford, this volume).

In metals or alloys where the host atoms carry localised magnetic moments, the muons experience both dipolar and contact hyperfine fields from these moments (Schenck, this volume). In non-metallic magnetic materials they usually experience only dipolar fields, unless there is a degree of covalency in the muon bonding which leaks some spin density onto the muon site. In either case, the local fields at the muon sites can be considerable - in the region 1–10kG for the hard magnets. The muon spin relaxation rate due to paramagnetic fluctuations then commonly falls within a measurable range, or even becomes embarrassingly fast!

Dynamic range

The dynamic range accessible to μSR measurements is about $0.1 < \lambda < 100\mu s^{-1}$ at a continuous muon source and $0.01 < \lambda < 10\mu s^{-1}$ at a pulsed source, say 4 orders of magnitude overall, centred roughly on the inverse muon lifetime:

$$0.01 < \lambda < 100\mu s^{-1}. \tag{46}$$

Of interest is the corresponding "window " on correlation times. Assuming the fast fluctuation limit, so that Equation 44 becomes

$$\lambda \approx (\gamma_\mu B_l)^2 \tau_c, \tag{47}$$

the window slides around according to the magnitude of B_l. As an example, for $B_l \approx 4$kG, (which is much larger than a typical nuclear local field such as $B_l \approx 4$G in Cu.) the

accessible range is

$$10^{-9} > \tau_c > 10^{-13}\text{s}, \tag{48}$$

which is appropriate to the paramagnetic region. The assumption of unique values for the correlation time and rms local field is adequate at sufficiently high temperatures, well into the paramagnetic phase, where the spins fluctuate independently at a rate given by the exchange constant: $\tau_c^{-1} \sim J$. On cooling towards the ordering transition, the fluctuations of individual moments become correlated and slow down, so that muon relaxation rate λ *increases*: a schematic temperature dependence for relaxation rate in magnetic materials is sketched in Figure 26. Equation 47 breaks down in the critical region close to the phase transition, however. The relaxation function remains exponential but a unique correlation time can no longer be defined, and a wave-vector dependent treatment is required, as it is for relaxation within the ordered phases (De Renzi, this volume).

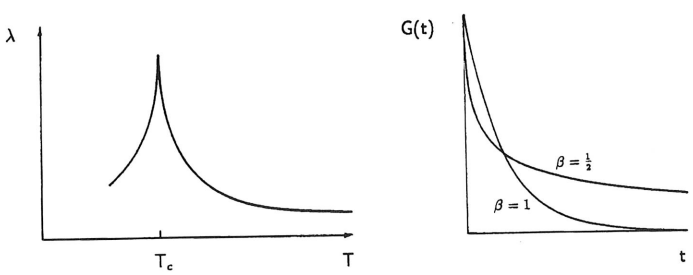

Figure 26. *Variation of relaxation rate with temperature in a magnetic material (a) and a comparison of simple and square-root exponential relaxation functions ($\beta = 1$ and $\beta = \frac{1}{2}$ in Equation 49).*

Energy conservation

In a given high field, muon, nuclear and electron spins are not "on speaking terms". The muon and nuclear Zeeman energies do not match and both are very much less than electron Zeeman energy. In systems of localised moments, the energy required to flip a muon or nuclear spin is most likely to be supplied by an electron flip-flop, *i.e* by the *difference* in energy between an upward and downward electron-spin transition, as in Figure 27(a). (The appropriate correlation time is then not necessarily the lifetime T_{1e} of the individual electron spin states but is likely to be much shorter.) In low fields (less than the local field), on the other hand, or under conditions of level crossing resonance, the muon and nuclear relaxation may be coupled as depicted in Figure 27(b). For itinerant systems, muon-electron flip-flops are permitted, the difference in their Zeeman energies being taken up by a change in kinetic energy of electrons near the Fermi energy.

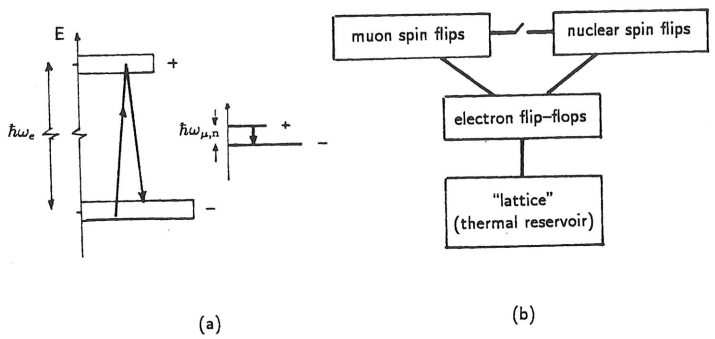

Figure 27. *Conservation of energy between muon or nuclear spin flips and electron spin flip-flops (a) and the resulting pathways for spin-lattice and cross relaxation (b). Direct cross relaxation to the host nuclei occurs only in low or zero field, or at a level crossing resonance.*

3.5 Other mechanisms

3.5.1 Spin-glasses: stretched exponentials

The BPP formulation results in simple exponential relaxation, as in Equation 38. In dilute magnetic systems and in spin-glasses, either τ_c or B_l in Equation 44 takes on a wide distribution of values. In effect, the relaxation rate λ then also takes on a distribution of values, so that a unique *relaxation time* T_1 cannot be defined. According to the weighting or distribution function, the superposition of exponential terms then commonly results in a *stretched exponential* form for the observed relaxation function:

$$G_{\parallel}(t) = \exp\{-(\lambda t)^{\beta}\}, \tag{49}$$

with $\beta < 1$. Values of the exponent in the range $\frac{1}{3} < \beta < 1$ are known in spin-glass systems (Uemura, Campbell this volume). The special case of $\beta = \frac{1}{2}$, which gives the "square-root exponential" function, $G_{\parallel}(t) = \exp\left[-\sqrt{\lambda t}\right]$, is compared with a simple exponential in Figure 26(b).

Note that setting $\beta = 2$ in Equation 49 gives a Gaussian, which is a reasonably good description of slow cross relaxation at low or zero field; reduction of β below 2 is a good indication of the onset of dynamics (with $\beta = 1$ describing the simple exponential of BPP mechanisms, of course).

3.5.2 Semiconductors: spin and charge exchange

In metals, the muon interacts with an indeterminate number of conduction electrons. In non-metals it is able to bind an individual electron to form *muonium*, which resembles atomic hydrogen; see also Roduner (this volume). An intermediate situation arises in highly-doped n–type semiconductors, where the muonium electron is involved in spin-flip encounters or *spin-exchange* with the extrinsic carriers. The depolarising effect is

transferred to the muon spin *via* the muonium hyperfine coupling. In the limit of fast fluctuation and low magnetic field, longitudinal relaxation rate is given by the simple expression

$$\lambda \sim (\pi \mathrm{A})^2/\nu, \tag{50}$$

where A is the muonium hyperfine constant and $\nu = \tau_c^{-1}$ the electron spin-flip rate; under other conditions the expressions are more complex, see *e.g.* Patterson, 1988.) The similar case of a muonated organic radical undergoing rapid spin exchange (*e.g.* in the gas phase, colliding with paramagnetic O_2 molecules) is treated by Senba (1994) and the extension to anisotropic muonium centres in n–type silicon is considered by Chow *et al.* (1994).

An equally powerful depolarisation mechanism is the so-called *charge-exchange* phenomenon in intrinsic semiconductors. This occurs at temperatures where muonium is nominally ionised, but can reform momentarily by capture and loss of conduction electrons.Hyperfine oscillations with a succession of uncorrelated electrons, illustrated in Figure 28, gives depolarisation rates reaching about $1\mu s^{-1}$ in Ge and $20\mu s^{-1}$ in Si.

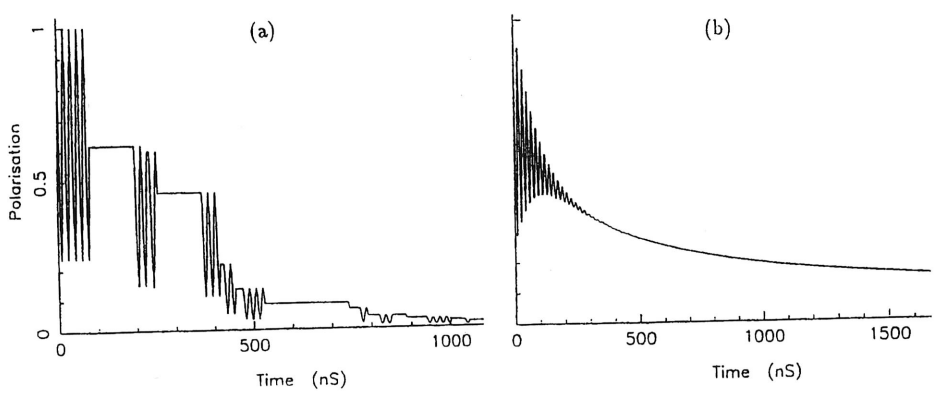

Figure 28. *Intermittent hyperfine coupling and its effect on the polarisation of a single muon (a) and an ensemble (b).*

In all these cases the rate of spin-exchange or charge-exchange of the muonium (or radical) electron is so fast that the muon *appears* to be in a diamagnetic state; that is, the muon spin rotation spectrum in transverse field would show precession at or near the Larmor frequency. The static average of the hyperfine interaction is negligible. (This despite the huge amplitude of the instantaneous or fluctuating field felt by the muon. Comparison of Equations 47 and 50 implies that this is equal to $\pi \mathrm{A}/\gamma_\mu$, which for muonium itself can be as large as 165kG! Even for an organic radical with A$\sim$300MHz it is about 11kG. (This is one definition of the "hyperfine field" but it should not to be confused with the more usual definition, $\pi \mathrm{A}/\gamma_e$, *i.e.* the effective field felt by the electron.) The fast fluctuation limit in Equation 50 requires $\nu \gg A$.)

The very different case of long-lived muonium spin states is treated in Section 3.6 below.

3.5.3 Polymers: 1D motion and the Risch–Kehr function

Figure 28 also describes the case of a muon incorporated into a polymer chain and experiencing a hyperfine interaction each time an unpaired electron spin comes within range (Jestädt *et al.* 1994). This probes the motion of any excitation carrying spin (whether charged or neutral) up and down the polymer chain. Muonium addition to the chain actually introduces such an excitation (Nagamine, this volume) but the same is true for intrinsic solitons or polarons.

The linear random walk executed by the electron spin cannot be described by the Lorentzian spectral density function of Equation 43 Instead, the electron revisits the muon at frequencies distributed according to:

$$J(\omega) \propto \sqrt{\omega}. \tag{51}$$

The result is a relaxation function specific to 1–D motion (Risch and Kerr 1992):

$$G_{\|}(t) = \exp(\Gamma t)\,\mathrm{erfc}(\sqrt{\Gamma t}). \tag{52}$$

This is similar in appearance to the square-root exponential (Figure 26b) but it tends to a $1/\sqrt{t}$ asymptote at long elapsed time – as does the probability of a 1–D random walker revisiting the starting point. Notice that since the relaxation is not exponential, a relaxation " rate" or "time" cannot be defined. If a fit to a simple exponential is forced, we find $\lambda \propto B^{-1/2}$ at high field, again mapping the spectral density function, but the fitted values are not independent of the data gate. More correctly, the parameter Γ becomes inversely proportional to field: $\Gamma \propto B^{-1}$.

3.6 Muonium-like systems

Before proceeding to the case of muonium and the muonated radicals, it is worth noting an alternative method of solving the simultaneous equations (8) for muons alone. We rewrite these in matrix form:

$$\begin{bmatrix} \dot{n}_+ \\ \dot{n}_- \end{bmatrix} = \begin{bmatrix} -W_\downarrow & W_\uparrow \\ W_\downarrow & -W_\uparrow \end{bmatrix} \begin{bmatrix} n_+ \\ n_- \end{bmatrix} \tag{53}$$

and call the 2×2 matrix the *relaxation matrix*. Using the standard algebraic method (a trial exponential solution), the relaxation *rate* is seen to be the non-zero eigenvalue of the relaxation matrix, given by

$$\begin{vmatrix} -W_\downarrow + \lambda & W_\uparrow \\ W_\downarrow & -W_\uparrow + \lambda \end{vmatrix} = 0, \tag{54}$$

i.e.

$$\lambda = (W_\downarrow + W_\uparrow) = T_1^{-1},$$

as in Equation 38. A sign convention has been adopted here so that the non-zero eigenvalue is positive. The apparently trivial second eigenvalue, $\lambda = 0$, is also important since it allows polarisation to relax to the steady thermal-equilibrium value.

The two-level diagram of Figure 22(a), and the 2×2 relaxation matrix of Equation 53, is valid for systems which display a (transverse field) muon spin rotation signal at the

muon Larmor precession frequency only. All interactions between the muons and other spins, whether nuclear or electronic, are taken to be fluctuating with significant amplitude but zero or negligible time-average. They induce transitions between the two levels but (with the exception of the Knight shift in metals) do not significantly displace them. Paramagnetic muonium states, on the other hand, are characterised by hyperfine and super-hyperfine interactions which greatly alter the energy levels and give rise to distinctive muon spin rotation or level-crossing spectra when the combined muon-electron spin eigenstates are reasonably long-lived; see also Roduner (this volume).This is true both for muonium itself as an interstitial trapped atom and for its open-shell molecular derivatives, *i.e.* the organic radicals. With electron, muon and possibly nuclear spins involved, the two-level model of Figure 22 is inadequate. In the following, we illustrate the problem with the four-level diagram for muonium, shown in Figure 29. This is valid for muonium itself and, with an appropriately smaller hyperfine constant, for a radical such as $C_{60}Mu$. ($C_{60}Mu$ is remarkable amongst species of such high molecular weight for comprising just two spins – that of the muon and that of the unpaired electron (here we neglect the ^{13}C nuclei, which have low abundance). Spin-lattice relaxation in $C_{60}Mu$ is described in Section 3.6.3. For most organic radicals, containing protons or other dipolar nuclei, a more complex energy level diagram is required – Roduner, this volume.)

3.6.1 The 4-level system

For the present purposes, the static (*i.e.* time average) hyperfine interaction is taken to be isotropic so that the zero-order Hamiltonian including Zeeman energy terms is, in a common notation,

$$\mathcal{H} = hA\,\mathbf{S}\cdot\mathbf{I} + \hbar\omega_e S_z + \hbar\omega_\mu I_z. \tag{55}$$

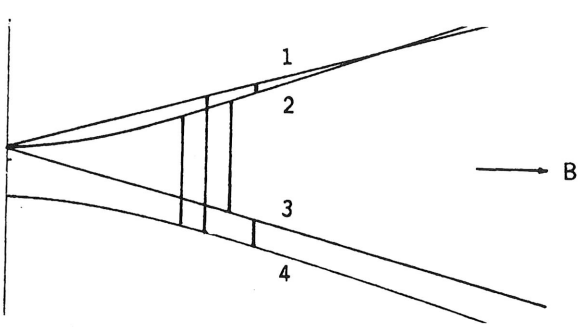

Figure 29. *Breit–Rabi energy level diagram for muonium or a simple muonated radical, with the transitions induced by fluctuations of a local field.*

Analytical expressions for the energy levels and eigenstates are given in the standard texts (*e.g.* Atherton, 1993); Figure 29 shows the energy levels schematically (sketched for an unphysically large value of γ_μ/γ_e.). Where the energy levels are linear in field, the simple product spin-states $|S_z, I_z\rangle$ are good eigenstates. So $|1\rangle = |++\rangle$ and $|3\rangle = |--\rangle$ are eigenstates at all fields. (This is no longer the case when the hyperfine interaction develops some static anisotropy. The triplet is then split in zero field and the high-field level crossing between states $|1\rangle$ and $|2\rangle$ is avoided.) The curvature of levels $|2\rangle$ and $|4\rangle$

indicate that these are field-dependent admixtures of $|+-\rangle$ and $|-+\rangle$. In the Paschen–Back region, *i.e.* at high field where the hyperfine interaction is essentially decoupled, state $|2\rangle$ approximates to $|+-\rangle$ with a small admixture, of order $2\pi A/\omega_e$, of $|-+\rangle$ and likewise state $|4\rangle$ approximates to $|-+\rangle$ with a small admixture of small $|+-\rangle$.

Motional perturbations induce transitions between the 4 levels, with different selection rules, different probabilities W_{ij} and different dependences on magnetic field according to mechanism. This is illustrated in Figure 29. Only rarely can separate "electron" or "nuclear" relaxation rates be defined, or identified with particular transition probabilities.

Without recourse to a full density matrix treatment, the problem of spin-lattice relaxation can be formulated in terms of simultaneous rate equations for the level populations (compare Equation 25):

$$\begin{bmatrix} \dot{n}_1 \\ \dot{n}_2 \\ \dot{n}_3 \\ \dot{n}_4 \end{bmatrix} = W \begin{bmatrix} -(W_{12}+W_{13}+W_{14}) & W_{21} & W_{31} & W_{41} \\ W_{21} & -(W_{21}+W_{23}+W_{24}) & W_{32} & W_{42} \\ W_{31} & W_{32} & -(W_{31}+W_{32}+W_{34}) & W_{43} \\ W_{41} & W_{42} & W_{43} & -(W_{41}+W_{42}+W_{43}) \end{bmatrix} \begin{bmatrix} n_1 \\ n_2 \\ n_3 \\ n_4 \end{bmatrix}. \tag{56}$$

τ_c is now the appropriate motional correlation time. We neglect for this purpose the difference between upward and downward probabilities, although Boltzmann factors may be included, of course. (The evaluation of the individual transition probabilities W_{ij} for different mechanisms, and the validity of the formulation, are described by Cox and Sivia (1997).)

The 4×4 matrix in Equation 56 is the relevant *relaxation matrix*. Since the total occupancy of the 4 levels is conserved by the transitions, $\sum_{i=1}^{4} n_i = 1$, this matrix has 3 non-zero eigenvalues. That is, the occupancy or population of each level evolves as a superposition of three exponentials. Again following standard algebraic methods, the general solution has the form

$$\begin{bmatrix} n_1(t) \\ n_2(t) \\ n_3(t) \\ n_4(t) \end{bmatrix} = A \begin{bmatrix} a_1 \\ a_2 \\ a_3 \\ a_4 \end{bmatrix} e^{-\lambda_A t} + B \begin{bmatrix} b_1 \\ b_2 \\ b_3 \\ b_4 \end{bmatrix} e^{-\lambda_B t} + C \begin{bmatrix} c_1 \\ c_2 \\ c_3 \\ c_4 \end{bmatrix} e^{-\lambda_C t} + D \begin{bmatrix} d_1 \\ d_2 \\ d_3 \\ d_4 \end{bmatrix}. \tag{57}$$

Here the column vectors are the eigenvectors of the relaxation matrix, the prefactors A, B, C are determined by the initial conditions and the constant term D by the thermal equilibrium condition. Analytical solutions may sometimes be obtained, *e.g.* in the limits of fast fluctuation and high temperature but, more generally, numerical solutions are required.

Note that an ESR pulse-saturation experiment would record the response of a population difference, $n_1 - n_4$, or $n_2 - n_3$ in which all three exponential terms of Equation 29 would be visible. For the particular case of μSR experiments, the observable quantity is not a population difference but the overall muon polarisation. The asymmetry in the muon decay in effect projects out and sums the expectation value from each of the four mixed electron-muon spin states (Cox, 1992):

$$P_z(t) = 2 \sum_{i=1}^{4} n_i(t) \langle i|I_z|i\rangle. \tag{58}$$

The factor 2 in Equation 58 converts spin to polarisation; it would be dropped if the Pauli spin operator σ_z were used instead of I_z.

In other words, pure muon spin relaxation is displayed even when there is coupling to electron spins, or indeed to other other nuclear spins: Equation 30 is readily extended to multispin systems. For the present 4–level model, one might expect to see a superposition of three exponential terms in the μSR response. They certainly all contribute but they appear in combinations such that, whenever the eigenvalues differ greatly in magnitude, only one of them has significant weight; alternatively, when the different eigenvalues have comparable weight, they have very similar magnitudes (Cox and Sivia, 1994). The muon relaxation function is in practice indistinguishable from a single exponential, therefore, which allows an effective relaxation rate $\lambda = \mathrm{T}_1^{-1}$ to be extracted from the simulations. (Multiple or stretched exponential relaxation, if observed, must be blamed on the presence of several distinct muonium centres or radical species, or on a distribution of parameters!) The characteristics for various relaxation mechanisms are considered below.

3.6.2 Muonium diffusion in non-metals

For muonium as for muons, motional perturbation of the magnetic environment may commonly be expressed as fluctuation of a local field. This is the case for atomic muonium diffusing interstitially through a solid lattice, where the local field B_l originates in the dipolar interaction with host spins and can change in magnitude or direction at each hop (Celio and Meier 1983). Five transitions are induced as depicted in Figure 29, with comparable strength at low field but very different strengths otherwise. In the high-field régime, the transitions $1\leftrightarrow4$ and $2\leftrightarrow3$ approximate to flips of the electron spin; they are induced strongly but are relatively ineffective for muon relaxation. The muon spin flips $1\leftrightarrow2$ and $3\leftrightarrow4$, on the other hand, though induced only weakly *via* the residual admixture of states $|+-\rangle$ and $|-+\rangle$, dominate the muon relaxation. It is interesting that whereas only transverse fluctuations cause spin-lattice relaxation in spin–$\frac{1}{2}$ systems, *longitudinal* fluctuations (*i.e.* fluctuations parallel to the applied or static-average field) are effective in hyperfine-coupled systems. These induce the flip-flop transitions $2\leftrightarrow4$.

The classic examples of this mechanism involve muonium diffusing interstitially in solids. They demonstrate various régimes of quantum diffusion, first observed in semiconductors and dielectrics and subsequently studied systematically in the rare gas solids and other cryocrystals see Storchak (this volume).

3.6.3 Muonated radicals

Mathematically equivalent is the case of muonated radicals in the gas phase, where the local field B_l originates in the coupling between the electron and muon spins and the angular momentum of the molecule. (This is known in molecular spectroscopy as the *spin-rotation* interaction – not to be confused with muon spin rotation!) The time dependence results from the molecular collisions, which jostle the angular momentum vector and change it in both magnitude and direction. μSR data for the muonated ethyl radical is significant in that no such complex species can be studied by ESR in the gas phase (Fleming *et al*, 1996).

For muonated radicals in condensed phases, other mechanisms take over. These are

motional perturbations of various components of the hyperfine interaction. Changes of vibrational state perturb the contact interaction, *i.e.* the isotropic component. (So the hyperfine "constant" is not in fact constant at all but fluctuates about its thermal average!) Only the flip-flop transition $2 \leftrightarrow 4$ is induced and this mechanism is ineffective in zero field, the spin-operator $\mathbf{S}\cdot\mathbf{I}$ being the same as that for the static-average contact interaction. Reorientation of the radical, in contrast, induces every possible transition in the Breit–Rabi diagram: this modulates the dipolar or anisotropic terms and fills every element of the 4×4 relaxation matrix. A similar mechanism can be effective for slightly anisotropic muonium diffusing in solids, so that relaxation is still seen even in solids such as quartz where the nuclear magnetism is weak or absent.

The various mechanisms can be recognised by their different field dependences of relaxation rate. Simulations are given in Figure 30. Relaxation by modulation of g-factor (*i.e.* spin-orbit coupling) would show an initial quadratic increase with applied field similar to that for modulation of contact interaction.

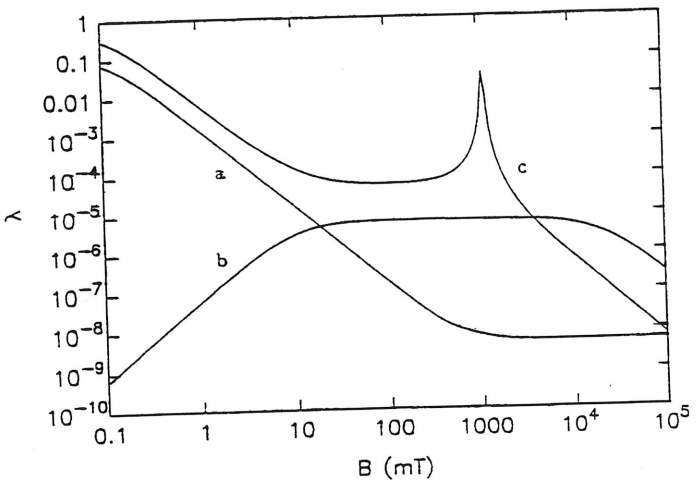

Figure 30. *Field dependences of longitudinal relaxation rate for muonium or muonated radicals, distinguishing fluctuation of a local field (a) and of isotropic (b) and anisotropic (c) components of the muon-electron hyperfine interaction.*

Experimental examples of the various mechanisms are reviewed and the data compared with model simulations by Cox (1998). One of the most fascinating cases is that of solid C_{60} fullerene, since in its plastic-crystal phases the individual bucky balls can reorient rapidly whilst remaining centred on their lattice sites. The mechanism gives a striking peak in relaxation rate, as in Figure 30c, centred on the level crossing. This is because anisotropic terms of the hyperfine coupling induce transitions $1 \leftrightarrow 2$ at all fields and the corresponding spectral density function $J(\omega_{12})$ peaks at the level crossing. Note that the level-crossing crossing condition is accessible for molecular radicals (typically falling below 2T) but not for atomic muonium (16T!). Data plus matching simulations are shown in Figure 31. The relaxation peak occurs even if the static average of the dipolar interaction is reduced to zero by the reorientation. So it should not be confused with the *level-crossing*

resonance, which is the oscillation and effective reduction of muon polarisation due to the static anisotropy, *i.e.* due to the mixing of spin states which avoids the crossing. Clearly the two phenomena are closely related, however, and in the simplest case the onset of reorientation broadens the resonance (Roduner, this volume). The resonant loss of polarisation measured by *integral counting* and the relaxation rate measured in the time domain then show the same Lorentzian field dependence with a width given by the reorientation rate. Under the conditions of Figure 31, the integral-counting resonances would probably be too broad to detect without baseline problems and the time-domain measurement becomes preferable.

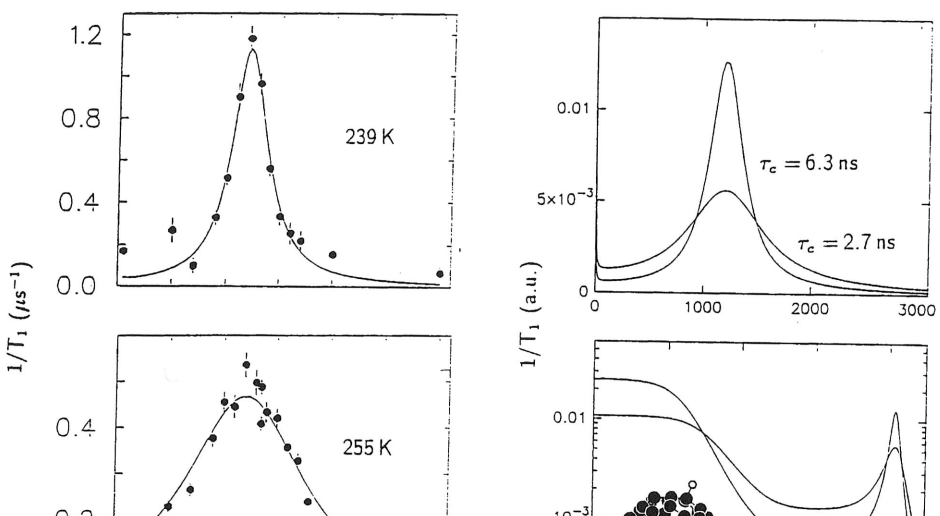

Figure 31. *Field dependence of longitudinal relaxation rate for the radical C_{60} Mu in solid C_{60} (Kiefl et al. 1992). The simulations use correlation times which match the data sets and also show (log. scale) the corresponding low-field relaxation (Cox, 1998).*

3.7 Concluding remarks

Muon spin-lattice relaxation in high fields is only significant if electron spins or atomic moments act as intermediaries. This creates an interesting link between dynamics and spectroscopy. When many electrons are involved, their own spin-states are short-lived, determined by their own spin-spin or spin-lattice interactions. We can then write hyperfine coupling to the muon as

$$\mathbf{I}\cdot\widetilde{\mathbf{A}}\cdot\mathbf{S}(t) = \mathbf{I}\cdot\widetilde{\mathbf{A}}\langle\mathbf{S}\rangle + \mathbf{I}\cdot\widetilde{\mathbf{A}}\cdot\mathbf{s}(t), \tag{59}$$

dividing it into static-average and fluctuating components. Ordered magnets are the obvious case where the static average term is large. In non-magnetic materials it reduces to a small Knight shift (metals) or paramagnetic shift (semiconductors) of the external field. This is a common situation in magnetic resonance and in μSR, namely that fluctuations of some interaction induce relaxation even when its time average is small or zero and spectral features associated with the interaction are unobservable. A 2-level representation of the muon spin-ensemble is adequate when the electron encounter rate or spin-flip rate is fast, imposed by the medium, and its depolarising effect is transferred to the muon *via* the hyperfine coupling.

For an isolated paramagnetic centre, however, the single-electron spin states are likely to be long-lived and we require the 4-level framework. It is now the hyperfine interaction which is time dependent, thanks to motion of the muonium centre or muonated radical:

$$\mathbf{I}\cdot\widetilde{\mathbf{A}}(t)\cdot\mathbf{S} = \mathbf{I}\cdot\langle\widetilde{\mathbf{A}}\rangle\cdot\mathbf{S} + \mathbf{I}\cdot\tilde{\mathbf{a}}(t)\cdot\mathbf{S}. \tag{60}$$

A significant static average term remains in this case, giving the characteristic frequencies in the transverse-field spectrum. The fluctuating components induce various transitions between the 4 levels, so causing spin-lattice relaxation both of the electron and the muon spins or, in low fields, of their combined spin states.

References

Abragam A, 1961, Principles of Nuclear Magnetism, *Oxford University Press.*

Addison-Jones, Percival P W, Brodovitch J-C, Ji F, Sharma D and Wlodek S, 1994, *Hyperfine Interactions* **87** 847–851.

Arseneau D J, Fleming D G, Senba M, Reid I D and Garner D M, 1988, *Canadian Journal of Chemistry* **66** 2018.

Atherton N M, 1993, Principles of Electron Spin Resonance, *Ellis Horwaood PTR Prentice hall Physical Chemistry series.*

Bloembergen N, Purcell E M and Pound R V, 1948, *Physical Review* **73** 679; see also standard magnetic resonance texts.

Brewer J H, Crowe K M, Gygax F N, Johnson R F, Patterson B D, Fleming D G and Schenck A, 1973, *Physical Review Letters* **31** 143–146.

Brewer J H, Spencer D P, Fleming D G and Coope J A R, 1981 Muonium hyperfine matrix in quartz, *Hyperfine Interactions* **8** 405–8.

Brewer J H, Kreitzman S R, Noakes D R, Ansaldo E J, Harshman D R and Keitel R, 1986, *Physical Review B* **33** 7813–6.

Briddon P R and Jones R, 1990, *Hyperfine Interactions* **64** 693–602.

Buttar D, Macrae R M, Webster B C and Roduner E, 1990, Solvent effects on the hyperfine coupling constant and barrier to internal rotation for the 2–muoxyprop–2–yl radical, *Hyperfine Interactions* **65** 927–936.

Celio M and Meier P F, 1983 *Physical Review B* **28** 39.

Chow K H, 1997, *Hyperfine Interactions* **105** 309–314.

Chow KH, Hitti B, Kiefl R F, Dunsiger S R, Lichti R L and Estle T L, 1996, *Physical Review Letters* **76** 3790–3793.

Chow K H, Kiefl R F, MacFarlane W A, Schneider J W, Cooke D W, Leon M, Paciotti M, Estle T L, Hitti B, Lichti R L, Cox S F J, Schwab C, Davis E A, Morrobel–Sosa A and Zavieh L, 1995, *Physical Review B* **51** 14762–14765.

Chow K H, Kiefl R F, Schneider J W, Hitti B, Estle T L, Lichti R L, Schwab C, DuVarney R C, Kreitzman S R, MacFarlane W A and Senba M, 1993, *Physical Review B* **47** 16004-16007.

Claxton TA, 1995, Mu@C_{70}: a theoretical study, *Philosophical Magazine B* 259–266.

Cooke D W, Leon M, Paciotti M A, Meier P F, Cox S F J, Davis E A, Estle T L, Hitti B, Lichti R L, Boekema C, Lam J, Morrobel–Sosa A and Oostens J, 1994, *Physical Review* B **50** 4391–4396.

Cox S F J, 1987, Implanted muon studies in condensed matter science, *Journal of Physics C: Solid State Physics* **21** 3187–3319.

Cox S F J, 1992, μSR studies of ice, illustrating the positive muon as a sensitive magnetic resonance probe of structure and dynamics, *Physica Scripta T* **45** 292–296.

Cox S F J, 1995, *Philosophical Transactions of the Royal Society of London A* **350** 171–185.

Cox S F J, 1998, *Solid State Nuclear Magnetic Resonance* **11** 103–121.

Cox S F J and Lichti R L, 1997, *Journal of Alloys and Compounds* **253–254** 414–419.

Cox S F J and Sivia D S, 1994, *Hyperfine Interactions* **87** 971.

Cox S F J and Sivia D S, 1997, *Applied Magnetic Resonance* **12** 213–226.

Cox S F J and Symons M C R, 1986, Molecular radical models for the muonium centres in semiconductors, *Chemical Physics Letters* **126** 516–525.

Davis E A, Singh A and Cox S F J, 1995, *Philosophical Transactions of the Royal Society of London A* **350** 227–236.

Fleming D G, Pan J J, Senba M, Arseneau D J, Kiefl R F, Shelley M Y, Cox S F J, Percival P W and Brodovitch J-C, 1996, *Journal of Chemical Physics* **105** 7517.

Füchslin R and Meier P F, 1994, *Hyperfine Interactions* **86** 741–746.

Hartmann O, Karlsson E, Norlin L-O, Niinikoskii T O, Kehr K H, Richter D, Welter J M, Yaouanc A and le Héricy J, 1980 *Physical Review Letters* **44** 337.

Iwanowski M, Maier K, Major J, Pfiz Th, Scheuermann R, Schimmele L, Seeger A and Hampele M, 1994, *Hyperfine Interactions* **86** 681–686.

Jestädt Th, Sivia D S and Cox S F J, 1997, *Hyperfine Interactions* **106** 45.

Kadono K, Kiefl R F, Brewer J H, Luke G M, Pfiz Th, Riseman T M and Sternlieb B J, 1990, *Hyperfine Interactions* **64** 635–640.

Kadono R, Macrae R M, Nagamine K and Nishiyama K, 1997, *Hyperfine Interactions* **105** 303–308.

Kadono R, Matsushita M, Macrae R M, Nishiyama K and Nagamine K, 1994, *Physical Review Letters* **73** 2724–2727.

Kiefl R F, Celio M, Estle T L, Kreitzman S R, Luke G M, Riseman T M and Ansaldo E J, 1988, *Physical Review Letters* **60** 224–226.

Kiefl R F, Percival P W, Brodovitch J-C, Leung S-K, Yu D, Venkateswaran K and Cox S F J, 1988, Measurement of ^{13}C hyperfine parameters of the cyclohexadienyl radical using muon level crossing resonance, *Chemical Physics Letters* **143** 613–618.

Kiefl R F, Schneider J W, Garner D M, Senba M, A.C. Gonzalez, Kempton J R, Arseneau D J, Venkateswaran K, Percival P W, Wei G, Wlodek S, Kojima K, Romanov W J, McCauley J P Jr., Coustel N, Fischer J E and Smith A B III, 1992, Molecular dynamics of MuC_{60} in solid C_{60}, *Physical Review Letters* **68** 1347.

Kiefl R F, Schneider J W, Keller H, Kündig W, Odermatt W, Patterson B D, Blazey K W, Estle T L and Rudaz S L, 1985, *Physical review B* **32** 530–532.

Kiefl R F, Schneider J W, MacFarlane A, Chow K H, Duty T L, Estle T L, Hitti B, Lichti R L, Ansaldo A J, Schwab C, Percival P W, Wei G, Wlodek S, Kojima K, Romanow W J, McCauley Jr. J P, Coustel N, Fischer J E and Smith III A B, 1992, *Physical Review Letters,* **68** 1347.

Kreitzman S R, Hitti B, Lichti R L, Estle T L and Chow K H, 1995, *Physical Review* B **51** 13117–13137.

R.L. Lichti, 1993 *Philosophical Transactions of the Royal Society of London A* **350** 323–333.

Lichti R L, Chow K H, Cooke D W, Cox S F J, Davis E A, DuVarney R A, Estle T L, Hitti B, Kreitzman S R, Macrae R M, Schwab C and Singh A, 1994 *Hyperfine Interactions* **86** 711–716.

Lichti R L, Chow K H, Cox S F J, Estle T L and Schwab C, 1997, *Materials Science Forum* **258–263** 179–184.

Lichti R L, Cox S F J, Schwab C, Estle T L and Chow K H, 1996, *Hyperfine Interactions* **105** 333-338.

Maric Dj M, Meier P F, Vogel S, Cox S F J, Davis E A and Schneider J W, 1991, *Journal of Physics: Condensed Matter Physics* **3** 9675–9686.

McKenna D, and Webster B, 1984, *Journal of the Chemical Society: Faraday Transactions* **80** 589 and 1985, **81** 225.

Meier P F, 1994 *Hyperfine Interactions* **86** 723–727.

Morton J R and Preston K F, 1978, Atomic parameters for paramagnetic resonance data, *Journal of Magnetic Resonance* **30** 577–582.

Patterson B D, 1988, *Review of Modern Physics* **60** 69–159.

Percival P W, Addison-Jones B, Brodovitch J-C, Ji F, Horoyski P J, Thewalt M L W and Anthony T R, 1995, ^{13}C hyperfine coupling constants in MuC_{60}, *Chemical Physics Letters* **245** 90-94.

Percival P W, Roduner E and Fischer H, 1978, Radiolysis effects in muonium chemistry, *Chemical Physics* **32** 353-367.

Percival P W, Brodovitch J-C, Leung S-K, Yu D, Kiefl R F, Garner D M, Arseneau D J, Fleming D G, Gonzalez A, Kempton J R, Senba M, Venkateswaran K and Cox S F J, 1989, Hyperfine constants for the ethyl radical in the gas phase, *Chemical Physics Letters*, **163**, 241–245.

Prassides K, Dennis T J S, Christides C, Roduner E, Kroto H W, Taylor R and Walton D R M, 1992, $Mu@C_{70}$: Monitoring the dynamics of fullerenes from inside the cage, *Journal of Chemical Physics* **96** 10600.

Ramos M J, McKenna D, Webster B C and Roduner E, 1984, *Journal of the Chemical Society: Faraday Transactions I* **80** 267.

Risch R and Kehr K W, 1992, *Physical Review B* **46** 5246.

Scheuermann R, 1997, *Thesis, University Stuttgart.*

Schneider J W, 1990, Thesis, University of Zurich and Schneider J W et al, 1990, *Hyperfine Interactions* **64** 543–550.

Slichter C P, 1963, 1990 (second edition) Principles of Magnetic Resonance, *Harper and Row, New York.*

Van de Walle C G, Denteneer P J H, Bar-Yam Y and Pantelides S T, 1989, *Physical Review B* **39** 10791–10808.

Webster B and Buttar D, *Journal of the Chemical Society: Faraday Transactions* **92** 2331.